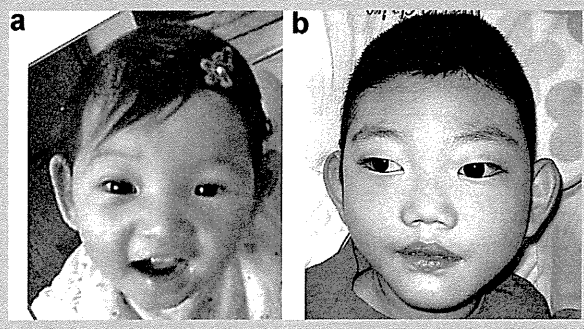

FIG. 2. Facial photograph of female Patient 11 (a) and male Patient 16 (b) showing an oval face, large eyes or irises, large ears, a broad nasal bridge, a broad nasal tip, and epicanthal folds.

DISCUSSION

This study revealed or confirmed several important clinical and radiological findings in Japanese patients with ID and MICPCH associated with *CASK* mutations. First, their head circumference at birth is within the normal range in about half, and birth height and weight are frequently normal; followed by postnatal growth retardation. Severe microcephaly develops usually within the first 4 months of life. Second, female patients acquire head control almost normally (between 3 and 6 months), but this is followed by motor delay. Third, more than half the female patients have epilepsy. In addition, MRI analyses showed that microcephaly and pontine and cerebellar hypoplasia develop in early infancy, and the corpus callosum is normal in size but appears large because the cerebrum is small. Finally, a male patient had a more severe clinical phenotype.

Microcephaly (−4 SD) and diminished body weight (−2 SD) became obvious after 4 months, while diminished stature (−2 to −3 SD) noted after 4 years. These findings are similar to those in a previous report of patients with *CASK* mutations in European countries [Moog et al., 2011]. MRI revealed that the area of the cerebrum is reduced in size after age 4 months, which was compatible with the OFC measurement. If MRI was performed in the neonatal period, it would confirm that the microcephaly observed in ID and MICPCH associated with *CASK* mutations predominantly develops postnatally. Therefore, the clinical diagnosis at birth may be difficult, and assessment of postnatal growth, especially OFC, is important in the diagnostic process.

The 15 females with *CASK* mutations developed head control normally or were mildly delayed, but had marked motor delay afterwards. A large majority (13/15) could sit alone between 7 and 25 months, but only 4/15 could walk without support between 2 and 6 years. This may be related to the fact that the cerebrum in neonates was often normal in size with no cerebral malformation on MRI. As 7 of 11 patients who could not walk at their most recent

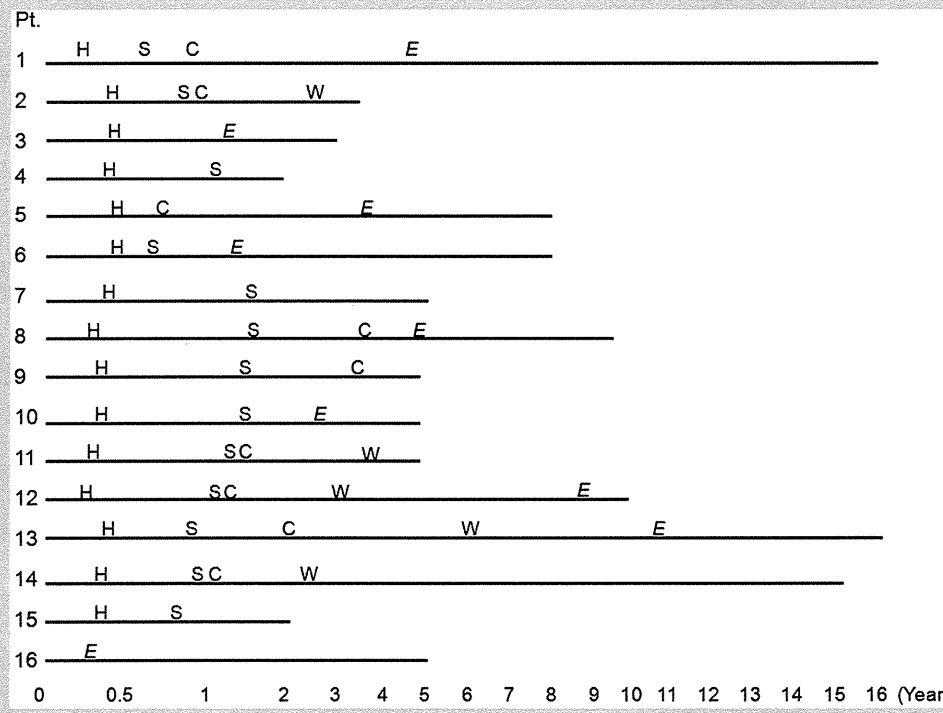

FIG. 3. Chart showing motor development and onset of epilepsy in patients with ID and MICPCH associated with *CASK* mutations. H, head control; C, crawl; S, sitting independently; W, walking independently; E, epilepsy.

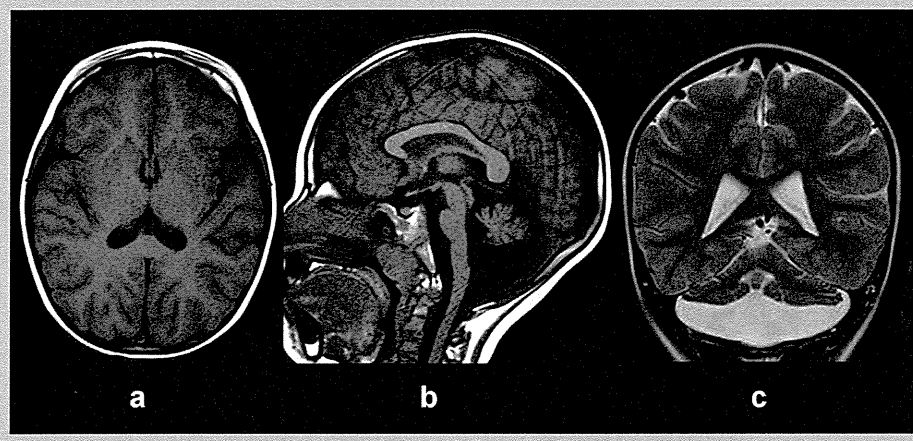

FIG. 4. Axial (a), mid-sagittal (b), and coronal MRI (c) of a 50-month-old female with *CASK* mutation (Patient 11). Note the microcephaly (a), hypoplastic pons (b), cerebellar hemispheres (c) and vermis (b) with normal appearance of the corpus callosum (a,b).

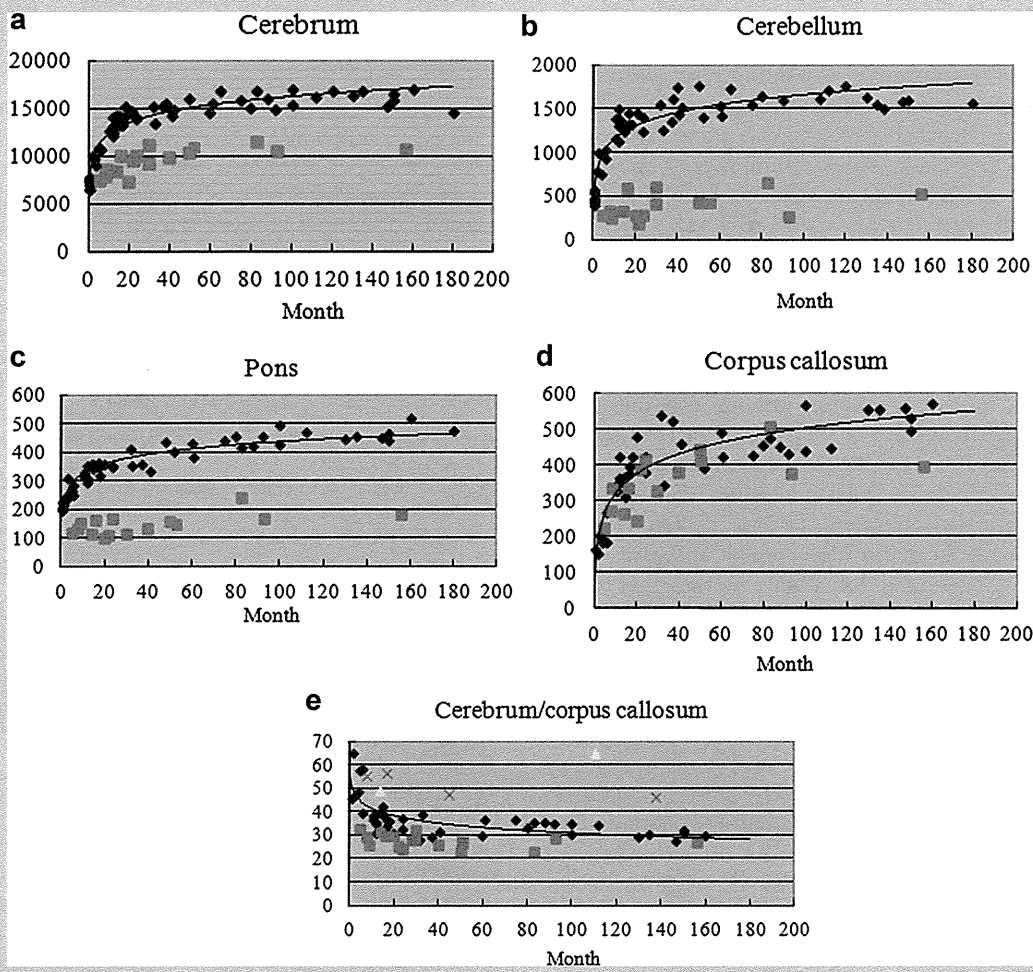

FIG. 5. Longitudinal changes in the cerebrum (a), cerebellar hemisphere (b), pons (c), and corpus callosum (d) areas, along with the cerebrum/corpus callosum area ratio (e). Diamonds represent control patients, squares patients with *CASK* mutations, triangles (e) the patient with PEHO syndrome, and Xs (e) the patients with other pontocerebellar malformations. The relatively normal callosal size combined with reduced size of other structures, resulting in the small cerebrum/corpus callosum ratio, appears to be a fairly unique characteristic of patients with *CASK* mutations.

evaluation were younger than 6 years, some might be expected to acquire this ability in the future.

Epilepsy was present in more than half of the females (53%) in this series, which is more frequent than the previously reported frequency (32%; 8/25) in European countries [Moog et al., 2011]. Seizure onset was between 17 and 130 months (mean, 60 months), and the epilepsy syndrome or seizure type was variable, similar to the previous report of onset at 1–8 years with various types of seizures [Moog et al., 2011]. Because most females without epilepsy were less than 6 years old, the frequency of epilepsy may be higher at subsequent re-evaluations. Child neurologists should be aware that epilepsy associated with ID and MICPCH due to *CASK* mutations has a relatively late onset. The neurological symptoms or facial features in the females were similar to those reported in European patients [Moog et al., 2011], however, hypohidrosis and hyposensitivity to pain were previously unrecognized. Although further clinical study is necessary to evaluate the frequency or severity of hypohidrosis and hyposensitivity to pain, ID and MICPCH associated with *CASK* mutations should be considered in the differential diagnosis of these symptoms.

The MRI findings in this case series confirmed the previous report of a normal to low-normal size of the corpus callosum and a low cerebrum/corpus callosum ratio with reduced areas of the cerebrum, pons, and cerebellar hemispheres. As five disease controls with pontine hypoplasia showed thinning of the corpus callosum and a high cerebrum/corpus callosum ratio, the normal size of the corpus callosum relative to a small cerebrum, which gives an impression of callosal thickening, is an important imaging clue for *CASK* mutations.

The growth pattern, neurologic development, neurological symptoms, and facial features were similar in the 15 females with loss-of-function mutations, which corresponds to previous reports showing that mutations resulting in a null allele are associated with a characteristic pattern of ID and MICPCH in females [Moog et al., 2011; Hayashi et al., 2012]. The one male in this study showed similar growth pattern, facial appearance, and MRI findings to the female patients; however, his neurologic manifestations were more severe, with no motor development and early onset, intractable epilepsy. Though it has been reported that *CASK* missense mutations in males can cause milder phenotypes, such as mild to severe ID with or without nystagmus, microcephaly, and/or dysmorphic features [Hackett et al., 2010] or FG syndrome [Piluso et al., 2009], their clinical features are distinct from ID and MICPCH. FG syndrome entails relative macrocephaly, agenesis of the corpus callosum, and mild ID with congenital nystagmus; microcephaly or cerebellar hypoplasia is rare. The striking difference in clinical severity between the two groups of *CASK* mutations might be explained by the different nature of the mutations; hypomorphic missense mutations in males are likely to have a relatively mild impact on protein structure and function, thus leading to less severe phenotype than the null mutations in females. Null mutations of *CASK* in males would be expected to cause a more severe phenotype than in female patients, usually resulting in prenatal or neonatal lethality. A partly penetrant *CASK* splice site mutation was reported in a severely affected male with MICPCH who died at 2 weeks [Najm et al., 2008]. In silico analysis in the present male patient with ID and MICPCH (Patient 16) showed the de novo missense mutation likely damaged and affected protein function with no splice site disruption, however, the functional CASK studies will be necessary to confirm the pathogenicity of this mutation. To clarify the details of clinical and radiologic features, it would be important to evaluate *CASK* in males with severe psychomotor delay and the characteristic facial appearance or MRI findings.

ACKNOWLEDGMENTS

We thank the patients and families for their contribution to this study.

REFERENCES

Hackett A, Tarpey PS, Licata A, Cox J, Whibley A, Boyle J, Rogers C, Grigg J, Partington M, Stevenson RE, Tolmie J, Yates JR, Turner G, Wilson M, Futreal AP, Corbett M, Shaw M, Gecz J, Raymond FL, Stratton MR, Schwartz CE, Abidi FE. 2010. CASK mutations are frequent in males and cause X-linked nystagmus and variable XLMR phenotypes. Eur J Hum Genet 18:544–552.

Hayashi S, Mizuno S, Migata O, Okuyama T, Makita Y, Hata A, Imoto I, Inazawa J. 2008. The *CASK* gene harbored in a deletion detected by array-CGH as a potential candidate for a gene causative of X-linked dominant mental retardation. Am J Med Genet Part A 146A:2145–2151.

Hayashi S, Okamoto N, Chinen Y, Takanashi J, Makita Y, Hata A, Imoto I, Inazawa J. 2012. Novel intragenic duplications and mutations of CASK in patients with mental retardation and microcephaly with pontine and cerebellar hypoplasia (MICPCH). Hum Genet 131:99–110.

Hsueh YP. 2006. The role of the MAGUK protein CASK in neural development and synaptic function. Curr Med Chem 13:1915–1927.

Hsueh YP. 2009. Calcium/calmodulin-dependent serine protein kinase and mental retardation. Ann Neurol 66:438–443.

Moog U, Kutsche K, Kortüm F, Chilian B, Bierhals T, Apeshiotis N, Balg S, Chassaing N, Coubes C, Das S, Engels H, Van Esch H, Grasshoff U, Heise M, Isidor B, Jarvis J, Koehler U, Martin T, Oehl-Jaschkowitz B, Ortibus E, Pilz DT, Prabhakar P, Rappold G, Rau I, Rettenberger G, Schlüter G, Scott RH, Shoukier M, Wohlleber E, Zirn B, Dobyns WB, Uyanik G. 2011. Phenotypic spectrum associated with CASK loss-of-function mutations. J Med Genet 48:741–751.

Najm J, Horn D, Wimplinger I, Golden JA, Chizhikov VV, Sudi J, Christian SL, Ullmann R, Kuechler A, Haas CA, Flubacher A, Charnas LR, Uyanik G, Frank U, Klopocki E, Dobyns WB, Kutsche K. 2008. Mutations of *CASK* cause an X-linked brain malformation phenotype with microcephaly and hypoplasia of the brainstem and cerebellum. Nat Genet 40:1065–1067.

Ninchoji J, Takanashi J. 2010. Pontine hypoplasia in 5p- syndrome; a key MRI finding for a diagnosis. Brain Dev 32:571–573.

Piluso G, D'Amico F, Saccone V, Bismuto E, Rotundo IL, Di Domenico M, Aurino S, Schwartz CE, Neri G, Nigro V. 2009. A missense mutations in *CASK* causes FG syndrome in an Italian family. Am J Hum Genet 84:162–177.

Takanashi J, Arai H, Nabatame S, Hirai S, Hayashi S, Inazawa J, Okamoto N, Barkovich AJ. 2010. Neuroradiological features of *CASK* mutations. AJNR Am J Neuroradiol 31:1619–1622.

Tanaka M, Tanaka Y, Hamano S, Nara T, Imai M. 1997. A case of PEHO (progressive encephalopathy with edema, hypsarrhythmia and optic atrophy) syndrome: Changes in clinical and neuroradiological findings. (In Japanese) No To Hattatsu 29:488–493.

RESEARCH ARTICLE

AMERICAN JOURNAL OF medical genetics PART A

MBTPS2 Mutation Causes BRESEK/BRESHECK Syndrome

Misako Naiki,[1,2] Seiji Mizuno,[3] Kenichiro Yamada,[1] Yasukazu Yamada,[1] Reiko Kimura,[1] Makoto Oshiro,[4] Nobuhiko Okamoto,[5] Yoshio Makita,[6] Mariko Seishima,[7] and Nobuaki Wakamatsu[1]*

[1]Department of Genetics, Institute for Developmental Research, Aichi Human Service Center, Kasugai, Aichi, Japan

[2]Department of Pediatrics, Nagoya University Graduate School of Medicine, Nagoya, Aichi, Japan

[3]Department of Pediatrics, Central Hospital, Aichi Human Service Center, Kasugai, Aichi, Japan

[4]Department of Pediatrics, Japanese Red Cross Nagoya Daiichi Hospital, Nagoya, Aichi, Japan

[5]Department of Medical Genetics, Osaka Medical Center and Research Institute for Maternal and Child Health, Izumi, Osaka, Japan

[6]Education Center, Asahikawa Medical University, Asahikawa, Hokkaido, Japan

[7]Department of Dermatology, Gifu University Graduate School of Medicine, Gifu, Gifu, Japan

Received 25 July 2011; Accepted 17 October 2011

BRESEK/BRESHECK syndrome is a multiple congenital malformation characterized by brain anomalies, intellectual disability, ectodermal dysplasia, skeletal deformities, ear or eye anomalies, and renal anomalies or small kidneys, with or without Hirschsprung disease and cleft palate or cryptorchidism. This syndrome has only been reported in three male patients. Here, we report on the fourth male patient presenting with brain anomaly, intellectual disability, growth retardation, ectodermal dysplasia, vertebral (skeletal) anomaly, Hirschsprung disease, low-set and large ears, cryptorchidism, and small kidneys. These manifestations fulfill the clinical diagnostic criteria of BRESHECK syndrome. Since all patients with BRESEK/BRESHECK syndrome are male, and X-linked syndrome of ichthyosis follicularis with atrichia and photophobia is sometimes associated with several features of BRESEK/BRESHECK syndrome such as intellectual disability, vertebral and renal anomalies, and Hirschsprung disease, we analyzed the causal gene of ichthyosis follicularis with atrichia and photophobia syndrome, *MBTPS2*, in the present patient and identified an p.Arg429His mutation. This mutation has been reported to cause the most severe type of ichthyosis follicularis with atrichia and photophobia syndrome, including neonatal and infantile death. These results demonstrate that the p.Arg429His mutation in *MBTPS2* causes BRESEK/BRESHECK syndrome. © 2011 Wiley Periodicals, Inc.

Key words: BRESEK/BRESHECK syndrome; IFAP syndrome; *MBTPS2*; mutation; S2P

How to Cite this Article:
Naiki M, Mizuno S, Yamada K, Yamada Y, Kimura R, Oshiro M, Okamoto N, Makita Y, Seishima M, Wakamatsu N. 2011. *MBTPS2* mutation causes BRESEK/BRESHECK syndrome.
Am J Med Genet Part A .

INTRODUCTION

BRESEK/BRESHECK syndrome (OMIM# 300404), a multiple congenital malformation disorder characterized by brain anomalies, intellectual disability, ectodermal dysplasia, skeletal deformities, Hirschsprung disease, ear or eye anomalies, cleft palate or cryptorchidism, and kidney dysplasia/hypoplasia [Reish et al., 1997]. The acronym BRESEK refers to the common findings, whereas BRESHECK refers to all manifestations. Because the first two patients were maternally related half brothers, an X-linked disorder was proposed. Although each symptom of these patients is often observed in other congenital diseases, the combination of all symptoms is rare, and only one additional patient with BRESEK has been reported to date [Tumialán and Mapstone, 2006]. Here, we present the fourth male patient with multiple anomalies. The patient presented with a variety of clinical features that were consistent with those of the previously reported BRESHECK syndrome.

The syndrome of ichthyosis follicularis with atrichia and photophobia (IFAP, OMIM# 308205), an X-linked recessive oculocutaneous disorder, is characterized by a peculiar triad of ichthyosis follicularis, total or subtotal atrichia, and varying degrees

Grant sponsor: Takeda Science Foundation; Grant sponsor: Health Labour Sciences Research Grant.
*Correspondence to:
Nobuaki Wakamatsu, Department of Genetics, Institute for Developmental Research, Aichi Human Service Center, 713-8 Kamiya-cho, Kasugai, Aichi 480-0392, Japan. E-mail: nwaka@inst-hsc.jp
Published online 00 Month 2011 in Wiley Online Library (wileyonlinelibrary.com).
DOI 10.1002/ajmg.a.34373

of photophobia [MacLeod, 1909]. Martino et al. [1992] reported a male patient with IFAP syndrome presented with short stature, intellectual disability, seizures, hypohidrosis, enamel dysplasia, congenital aganglionic megacolon, inguinal hernia, vertebral and renal anomalies, and the classic symptom triad of IFAP syndrome. This report broadened the clinical features of IFAP syndrome. It should be noted that the clinical symptoms of this patient are quite similar to those of BRESHECK syndrome, with the exception of cleft palate, cryptorchidism, and photophobia (Patient 5; Table I). The gene mutated in patients with IFAP syndrome, *MBTPS2* (GenBank reference sequence NM_015884), was identified from a variety of clinical features of IFAP syndrome, including the triad and neonatal death [Oeffner et al., 2009]. Thus, the mode of inheritance and several clinical features are common to both BRESEK/BRESHECK and IFAP syndromes. These findings prompted us to perform mutation analysis of *MBTPS2* in the present patient, resulting in the identification of a missense mutation.

MATERIALS AND METHODS

Patients

Written informed consent was obtained from the parents of the patient. Experiments were conducted after approval of the institutional review board of the Institute for Developmental Research, Aichi Human Service Center. The patient (II-1; Fig. 3) was born to a 31-year-old mother (I-2) and a 31-year-old father (I-1), both healthy Japanese individuals without consanguinity. His mother miscarried her first child at 5 weeks. The pregnancy of the patient reported here was complicated with mild oligohydramnios, and he was delivered by caesarean because of a breech position at 38 weeks of gestation. His birth weight was 1,996 g (−2.6 SD), and he measured 44 cm (−2.6 SD) in length with an occipitofrontal circumference of 32.5 cm (−0.5 SD). Apgar scores at 1 and 5 min were four and eight, respectively. The patient exhibited generalized alopecia and lacked eyelashes, scalp hair, and eyebrows (Fig. 1A). The skin on the entire body was erythematous with

TABLE I. Clinical Features of BRESEK/BRESHECK and IFAP Syndromes and *MBTPS2* Mutation

	BRESEK/BRESHECK syndrome				IFAP syndrome		
Patient	**1**	**2**	**3**	**4**	**5**	**6**	**7**
Clinical features							
Gender	M	M	M	M	M	M	M
Gestational age (weeks)	32	40	ND	38	30	ND	ND
Birth weight (g)	990	2,230	ND	1,996	2,040	ND	ND
Intrauterine growth retardation	+	+	ND	+	−	ND	ND
Major features							
Follicular ichthyosis	−	−	ND	−	+	+	+
Atrichia	+	+	+	+	+	+	+
Photophobia	−	−	−	+	+	+	+
Brain malformation	+	+	+	+	+	−	+
Mental and growth retardation	+	+	+	+	+	+	+
Skeletal (Vertebrate) anomalies	+	+	+	+	+	+	+
Hirschsprung disease	−	+	+	+	+	+	+
Eye malformation or	+	+	+	−	+	−	−
Large ears	+	+	+	+	+	−	−
Cleft lip/palate or	−	+	−	−	−	+	−
Cryptorchidism	+	+	−	+	−	−	−
Kidney malformation	+	+	−	+	+	+	+
Other features							
Microcephaly	+	+	+	+	+	−	+
Seizures	−	+	+	+	+	−	+
Deafness	−	+	−	+	−	−	−
Hand anomalies	+	+	+	−	+	+	+
Cardiac anomalies	−	−	+	−	−	−	+
Inguinal hernia	−	−	−	−	+	+	+
Trachea anomalies	−	−	−	+	−	−	−
Regression	−	−	−	+	−	−	−
Age	6 h d	7 y	1.5 y	8 y	3 y	9 m d	14 m d
MBTPS2 mutation	NP	NP	NP	R429H	NP	R429H	R429H

+, present;−, not present; M, male; ND, not described; NP, not performed; h, hour; d, dead; m, month; y, year; R429H, Arg429His; BRESEK/BRESHECK syndrome, [Patients 1-4]; IFAP syndrome, [Patients 5–7]; Patients: 1, Reish et al. [1997] patient 1; 2, Reish et al. [1997] patient 2; 3, Tumialán and Mapstone [2006]; 4, present case; 5, Martino et al. [1992]; 6, Oeffner et al. [2009] 3-III:3; 7, Oeffner et al. [2009] 3-III:4.

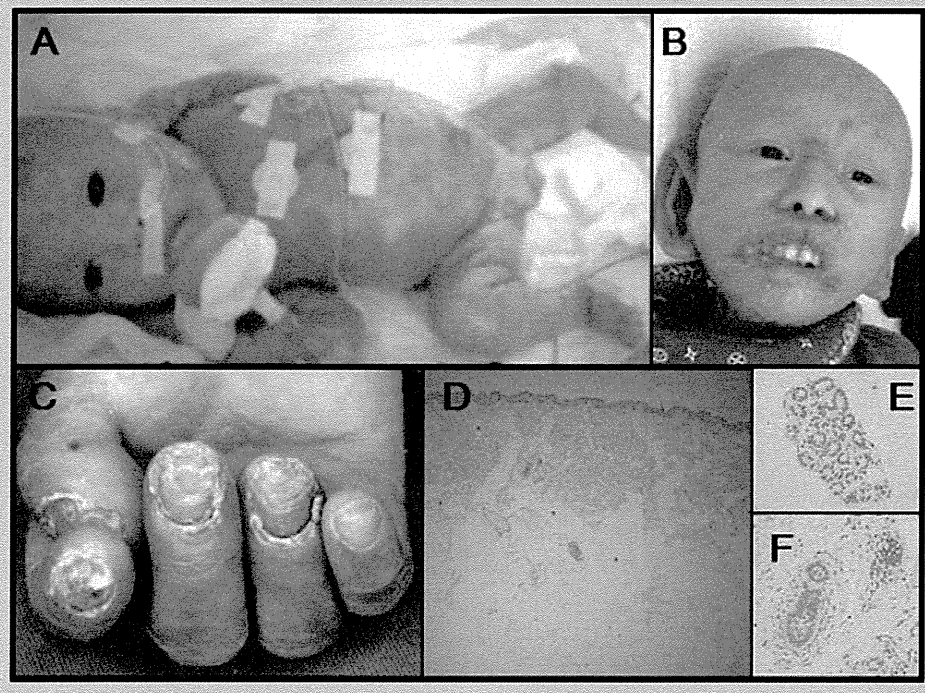

FIG. 1. Clinical appearance and dermatological findings of the patient. A: Lateral view of the patient at birth. Note the generalized alopecia with an absence of scalp hair, eyebrows, and eyelashes. The skin was dry and scaly, and an itchy erythema was observed over the entire body. B: Frontal view of the patient at 4 years of age. Note the characteristic facial appearance with long, malformed ears, a relatively high nasal bridge, and a wide nasal base. C: The patient had normal-sized but deformed and thickened nails. D–F: Histologic examination of the abdominal skin at the age of 15 months showed a reduced number of hair follicles (D), normal eccrine glands (E), and hypoplastic hair follicles (F).

continuous desquamation (Fig. 1A). He had malformed large ears, an inferiorly curved penis, and a bifid scrotum. The testicles were not palpable. He experienced persistent constipation, and total colonic Hirschsprung disease was confirmed through barium enema (Fig. 2E) and rectal biopsy at 2 months. A bone survey performed using three-dimensional (3D) computed tomography (CT) showed abnormal imbalanced hemivertebrae in the two lowest thoracic vertebral bodies (Fig. 2C). The patient's right kidney was smaller than normal. Brain magnetic resonance imaging (MRI) at 3 years of age demonstrated decreased volumes of the frontal and parietal lobes and thinning of the corpus callosum with dilatation of the ventricles (Fig. 2A,B). There were no abnormalities of the eyes or optic nerves. We concluded that the patient had BRESHECK syndrome. The patient had seizures at 5 months of age with an apneic episode and cyanosis. Electroencephalographic (EEG) analysis showed abnormal patterns of sharp waves in the posterior lobe. The seizures were almost completely controlled with phenobarbital. The patient was allergic to milk. At 7 months, tracheal endoscopy revealed subglottic tracheal stenosis and abnormal segmentation of the left lung. A chest CT performed at 3 years of age showed a congenital cystic adenomatoid malformation (CCAM) in the right upper lobe (Fig. 2D). Auditory brain stem responses showed bilateral 80 dB hearing loss at 8 months of age.

The patient exhibited delayed psychomotor development during his infancy. He could drink from a bottle at the age of 3 months and could sit up unsupported at 15 months. Abdominal skin biopsy at 15 months revealed reduced number of hair follicles (Fig. 1D). The eccrine glands were normal (Fig. 1E), and most of his hair follicles appeared to be hypoplastic (Fig. 1F). These findings were similar to ichthyosiform erythroderma. Photophobia was noted when the patient left the hospital and first went outside at 18 months of age. At 2 years and 6 months of age, he had a series of epileptic episodes. He experienced a maximum of 100 seizures per day, and EEG analysis showed continual abnormal spikes in the posterior lobe. The seizures were controlled with clonazepam therapy. At 2 years and 9 months of age, he could stand with support and displayed social smiles when interacting with other people. However, the patient developed psychomotor regression at the age of 3 years. He exhibited a progressive loss of emotional response to others, developed hypotonia, and could not stand or sit alone. At 4 years of age, he became bedridden and showed almost no response to people. He had highly desquamated skin, similar to that seen in ichthyosis (Fig. 1B), and easily developed erythema on the skin of the entire body. The patient had deformed and thickened nails (Fig. 1C). He had persistent corneal erosions, but ophthalmoscopy could not be performed at the age of 4 years because of corneal opacification.

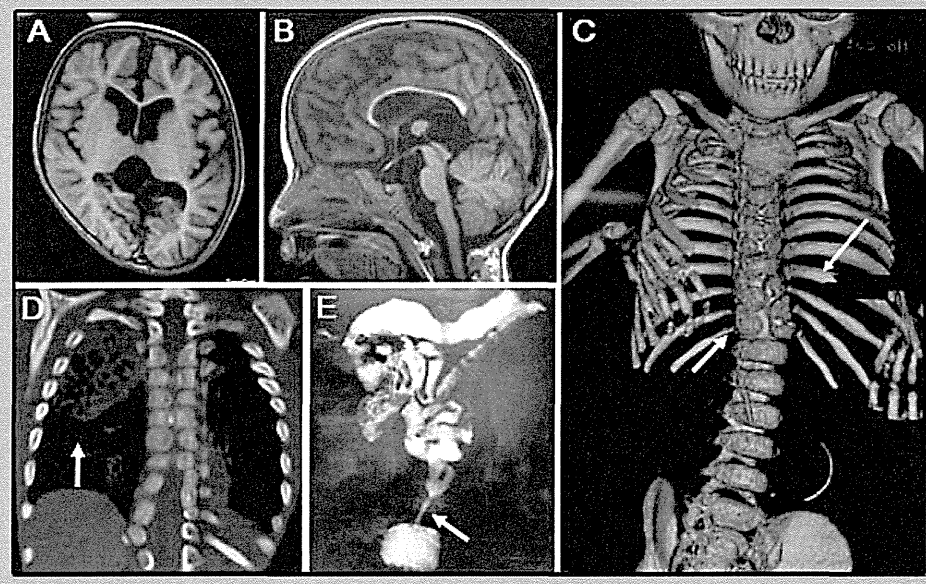

FIG. 2. CT and MRI findings of the patient. A,B: Brain MRI (T1-weighted image) at 3 years of age showed decreased volume of the cortex in the frontal and parietal lobes, the presence of a subdural cyst in the corpora quadrigemina, and dilatation of the lateral and fourth ventricle. C: A bone survey performed using 3D CT showed abnormal segmentation of the ninth rib and an imbalanced hemivertebrae in the two lowest thoracic vertebral bodies (shown with arrows). D: CT of the chest showed CCAM (indicated by the arrow) in the right upper lobe. E: Barium enema showed a reduced caliber rectum (indicated by the arrow), suggesting that the patient had Hirschsprung disease.

Chromosomal and Molecular Genetic Studies

Genomic DNA isolated from the patient's peripheral white cells by phenol/chloroform extraction was used for *MBTPS2* mutation analysis. PCR-amplified DNA fragments were isolated using the QIAEX II Gel Extraction Kit (Qiagen, Valencia, CA) and purified using polyethylene glycol 6000 precipitation. PCR products were sequenced with the Big Dye Terminator Cycle Sequencing Kit V1.1 and analyzed with the ABI PRISM 310 Genetic Analyzer (Life Technologies, Carlsbad, CA). We also performed G-banded chromosome analysis at a resolution of 400–550 bands, genome-wide subtelomere fluorescence in situ hybridization (FISH) analysis, and array comparative genomic hybridization (array CGH) using Whole Human Genome Oligo Microarray Kits 244K (Agilent Technologies Inc., Palo Alto, CA) to identify genomic abnormalities.

RESULTS

G-banded chromosome analysis and genome-wide subtelomere FISH analyses did not show chromosomal rearrangements in the patient. Array CGH analysis did not show copy number changes in the patient's genome with the exception of known copy-number variations (CNVs). Since some patients with IFAP syndrome have been reported to present with several clinical features of BRESEK/BRESHECK syndrome, including severe intellectual disability, vertebral and renal anomalies, and Hirschsprung disease, we conducted a comprehensive sequencing analysis of all exons and intron–exon boundaries of *MBTPS2*. This analysis identified a missense mutation (c.1286G>A, [p.Arg429His]) in exon 10, which was previously reported for IFAP syndrome (Fig. 3). The mutation was also found in one allele of the mother (I-2), indicating that the mutation was of maternal origin and that the mother was a heterozygous carrier (Fig. 3).

DISCUSSION

In this report, we describe the fourth male patient with BRESHECK syndrome in whom we identified a missense mutation (c.1286G>A, [p.Arg429His]) in *MBTPS2*, which is the causal gene for IFAP syndrome. *MBTPS2* encodes a membrane-embedded zinc metalloprotease, termed site-2 protease (S2P). S2P cleaves and activates cytosolic fragments of sterol regulatory element binding proteins (SREBP1 and SREBP2) and a family of bZIP membrane-bound transcription factors of endoplasmic reticulum (ER) stress sensors (ATF6, OASIS), after a first luminal proteolytic cut by site-1 protease (S1P) within Golgi membranes [Sakai et al., 1996; Ye et al., 2000; Kondo et al., 2005; Asada et al., 2011]. The SREBPs control the expression of many genes involved in the biosynthesis and uptake of cholesterol, whereas ATF6 and OASIS induce many genes that clean up accumulated unfolded proteins in the ER. Dysregulated SREBP activation, impaired lipid metabolism, and accumulation of unfolded proteins in the ER caused by *MBTPS2* mutations could lead to disturbed differentiation of epidermal structures, resulting in the symptom triad of IFAP syndrome [Cursiefen et al., 1999; Traboulsi et al., 2004; Elias et al., 2008]. Oeffner et al. [2009] first identified five missense mutations in *MBTPS2* in patients with IFAP

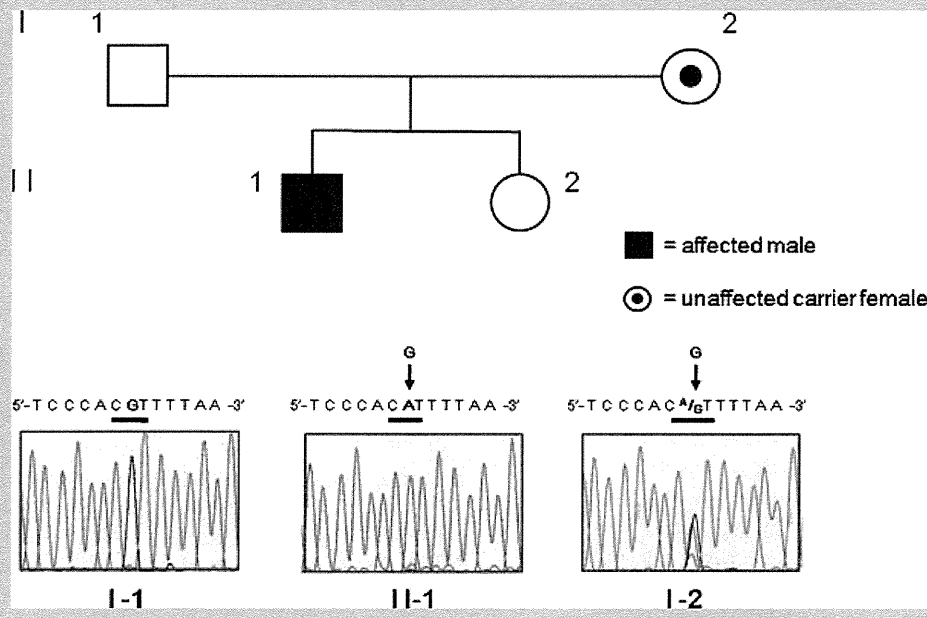

FIG. 3. Identification of a disease mutation. The sequence analyses of the patient (II-1) showed a c.1286G>A variant in exon 10 of *MBTPS2*, which predicts p.Arg429His, as indicated by the arrow (middle panel). The mother (I-2) was heterozygous for the mutation ($C^A/_GT$) (right panel).

syndrome. Transfection studies using wild type and mutant *MBTPS2* expression constructs demonstrated that the five *MBTPS2* mutations did not affect S2P protein amount and localization in the ER. However, enzyme activities, as measured by sterol responsiveness, were decreased in S2P-deficient M19 cells when the mutant *MBTPS2* was transiently expressed. Interfamilial phenotypic differences between male IFAP patients and the properties of mutants in functional assays predict a genotype–phenotype correlation, ranging from mild forms of the triad with relatively high enzyme activity (~80%) to severe manifestations of intellectual disability, various developmental defects, and early death with low enzyme activity (~15%). The identified p.Arg429His mutation in the patient reported here is one of the five missense mutations with the lowest enzyme activity. It was previously reported that all four patients harboring the p.Arg429His mutation died within 14 months of birth. The five mutations were not located in the HEIGH motif (amino acids [aa] 171–175) or in the $LD_{467}G$ sequence, both of which are regions important for coordinating the zinc atom at the enzymatic active site for protease activity in the Golgi membrane [Zelenski et al., 1999]. However, among the five mutations, the p.Arg429His mutation is located closest to the intramembranous domain, and it strongly reduced the enzymatic activity and caused a severe phenotype. This finding suggests that mutations in the HEIGH motif or in the $LD_{467}G$ sequence are fatal because they lead to a null function of the S2P. Although the detailed skin findings of the four patients with the p.Arg429His mutation have not been reported, it should be noted that one of the four patients (3-III:4) with the p.Arg429His mutation had brain anomaly, seizures, psychomotor retardation, vertebrae anomaly, Hirschsprung disease, absence of a kidney, atrial septum defect, and inguinal hernia, in addition to the symptom triad of IFAP syndrome [Oeffner et al., 2009]. These symptoms overlap with the majority of symptoms observed in BRESHECK syndrome (BRESHK; six of eight symptoms observed in BRESHECK) (Table I), and the present patient has BRESHECK syndrome. Collectively, these observations suggest that the most severe form of the syndrome caused by the p.Arg429His mutation in *MBTPS2* shows features quite similar or identical to those of BRESEK/BRESHECK syndrome.

There are two major differences in the definitions of IFAP syndrome and BRESEK/BRESHECK syndrome. Ichthyosis follicularis, one of the triad symptoms of IFAP syndrome, is a clinical condition of the skin. However, several studies on IFAP syndrome have reported various skin eruptions such as psoriasis-like and ichthyosis-like eruptions [Martino et al., 1992; Sato-Matsumura et al., 2000]. In contrast, patients with BRESEK/BRESHECK syndrome showed severe lamellar desquamation with diffuse scaling [Reish et al., 1997], similar to that observed in the present patient. This could be because of the difference in features of the skin, namely, ichthyosiform erythroderma-like appearance versus ichthyosis follicularis, in patients with the most severe forms of *MBTPS2* mutation and patients with IFAP syndrome who were described earlier, respectively.

The second difference is that photophobia was not described in the reported three male patients with BRESEK/BRESHECK syndrome [Reish et al., 1997; Tumialán and Mapstone, 2006]. In the present patient, photophobia became evident after he was diagnosed with BRESHECK syndrome. Photophobia is a symptom of epithelial disturbances of the cornea, such as ulceration and vascularization, which result in corneal scarring [Traboulsi et al., 2004]. In the most severe cases of *MBTPS2* mutation, such as

patients with severe intellectual disability who are bedridden and die early, it is likely that the patients were treated in the hospital without being exposed to sunlight. Therefore, it would be difficult to observe photophobia as a main symptom in those cases. Moreover, two previously described patients with BRESEK/BRESHECK syndrome had initial maldevelopment of one eye or small optic nerves. In these patients, photophobia may not have been obvious because of malformations of the eyes and optic nerves [Reish et al., 1997]. In our study, the patient showed clinical features of BRESHECK syndrome and photophobia with *MBTPS2* mutation, indicating that the clinical features of the present patient are extremely broad compared to the features of IFAP syndrome caused by *MBTPS2* mutation that have been previously reported [MacLeod, 1909].

Recently, a missense mutation (c.1523A>G, [p.Asn508Ser]) in *MBTPS2* was identified from 26 cases of three independent families with keratosis follicularis spinulosa decalvans (KFSD; OMIM# 308800), which is characterized by the development of hyperkeratotic follicular papules on the scalp followed by progressive alopecia of the scalp, eyelashes, and eyebrows in addition to childhood photophobia and corneal dystrophy [Aten et al., 2010]. A significant association was found between KFSD and the p.Asn508Ser mutation. The specific localization of alopecia to the scalp, eyelashes, and eyebrows and the limited childhood photophobia of KFSD indicate that KFSD has a relatively mild phenotype. The authors postulate that IFAP syndrome and KFSD are within the spectrum of one genetic disorder with a partially overlapping phenotype and propose that a new name should be chosen for KFSD/IFAP syndrome with an *MBTPS2* mutation. In contrast, the BRESHECK syndrome observed in the present patient has a severe phenotype caused by the p.Arg429His mutation. The present patient and the two patients (3-III:3 and 3-III:4) with the p.Arg429His mutation displayed broader clinical features, including eight features (BRESHECK) and six features (RESHCK and BRESHK) of BRESEK/BRESHECK syndrome, respectively (patients 4, 6, and 7; Table I) [Oeffner et al., 2009]. There is a debate regarding whether the two patients harboring six features were correctly diagnosed with BRESEK/BRESHECK syndrome since the patients did not have "BRESEK" but rather a combination of six other clinical features. To better understand and clearly distinguish the clinical features of the present patient from those of the reported patients with *MBTPS2* mutations, we propose the nomenclature of "BRESHECK/IFAP syndrome" for the present patient because he has clinical features of BRESHECK syndrome. We also suggest that the BRESHECK/IFAP syndrome be used for a broader definition that would include patients harboring most features of BRESHECK syndrome, including the previously reported two patients (3-III:3 and 3-III:4) with p.Arg429His mutation in *MBTPS2* [Oeffner et al., 2009]. Data from further genetic and clinical studies on more patients are required to determine which genes or *MBTPS2* mutations are associated with BRESEK/BRESHECK or BRESHECK/IFAP syndrome, respectively.

ACKNOWLEDGMENTS

We thank the patient and his family for participating in the study. This study was supported by the Takeda Science Foundation (to N.W.) and by the Health Labour Sciences Research Grant (to S.M. and N.W.).

REFERENCES

Aten E, Brasz LC, Bornholdt D, Hooijkaas IB, Porteous ME, Sybert VP, Vermeer MH, Vossen RH, van der Wielen MJ, Bakker E, Breuning MH, Grzeschik KH, Oosterwijk JC, den Dunnen JT. 2010. Keratosis follicularis spinulosa decalvans is caused by mutations in MBTPS2. Hum Mutat 31:1125–1133.

Asada R, Kanemoto S, Kondo S, Saito A, Imaizumi K. 2011. The signalling from endoplasmic reticulum-resident bZIP transcription factors involved in diverse cellular physiology. J Biochem 149:507–518.

Cursiefen C, Schlötzer-Schrehardt U, Holbach LM, Pfeiffer RA, Naumann GOH. 1999. Ocular findings in ichthyosis follicularis, atrichia, and photophobia syndrome. Arch Ophthalmol 117:681–684.

Elias PM, Williams ML, Holleran WM, Jiang YJ, Schmuth M. 2008. Pathogenesis of permeability barrier abnormalities in the ichthyoses: Inherited disorders of lipid metabolism. J Lipid Res 49:697–714.

Kondo S, Murakami T, Tatsumi K, Ogata M, Kanemoto S, Otori K, Iseki K, Wanaka A, Imaizumi K. 2005. OASIS, a CREB/ATF-family member, modulates UPR signalling in astrocytes. Nat Cell Biol 7:186–194.

MacLeod JMH. 1909. Three cases of 'ichthyosis follicularis' associated with baldness. Br J Dermatol 21:165–189.

Martino F, D'Eufemia P, Pergola MS, Finocchiaro R, Celli M, Giampà G, Frontali M, Giardini O. 1992. Child with manifestations of dermotrichic syndrome and ichthyosis follicularis alopecia photophobia (IFAP) syndrome. Am J Med Genet 44:233–236.

Oeffner F, Fischer G, Happle R, König A, Betz RC, Bornholdt D, Neidel U, Boente Mdel C, Redler S, Romero-Gomez J, Salhi A, Vera-Casaño A, Weirich C, Grzeschik KH. 2009. IFAP syndrome is caused by deficiency in MBTPS2, an intramembrane zinc metalloprotease essential for cholesterol homeostasis and ER stress response. Am J Hum Genet 84:459–467.

Reish O, Gorlin RJ, Hordinsky M, Rest EB, Burke B, Berry SA. 1997. Brain anomalies, retardation of mentality and growth, ectodermal dysplasia, skeletal malformations, Hirschsprung disease, ear deformity and deafness, eye hypoplasia, cleft palate, cryptorchidism, and kidney dysplasia/hypoplasia (BRESEK/BRESHECK): New X-linked syndrome? Am J Med Genet 68:386–390.

Sakai J, Duncan EA, Rawson RB, Hua X, Brown MS, Goldstein JL. 1996. Sterol-regulated release of SREBP-2 from cell membranes requires two sequential cleavages, one within a transmembrane segment. Cell 85: 1037–1046.

Sato-Matsumura KC, Matsumura T, Kumakiri M, Hosokawa K, Nakamura H, Kobayashi H, Ohkawara A. 2000. Ichthyosis follicularis with alopecia and photophobia in a mother and daughter. Br J Dermatol 142:157–162.

Traboulsi E, Waked N, Mégarbané H, Mégarbané A. 2004. Ocular findings in ichthyosis follicularis–alopecia–photophobia (IFAP) syndrome. Ophthal Genet 25:153–156.

Tumialán LM, Mapstone TB. 2006. A rare cause of benign ventriculomegaly with associated syringomyelia: BRESEK/BRESHECK syndrome. Case illustration. J Neurosurg 105:155.

Ye J, Rawson RB, Komuro R, Chen X, Davé UP, Prywes R, Brown MS, Goldstein JL. 2000. ER stress induces cleavage of membrane-bound ATF6 by the same proteases that process SREBPs. Mol Cell 6:1355–1364.

Zelenski NG, Rawson RB, Brown MS, Goldstein JL. 1999. Membrane topology of S2P, a protein required for intramembranous cleavage of sterol regulatory element-binding proteins. J Biol Chem 274:21973–21980.

Journal of Human Genetics (2012) 57, 580–586

www.nature.com/jhg

ORIGINAL ARTICLE

Reduced *PLP1* expression in induced pluripotent stem cells derived from a Pelizaeus–Merzbacher disease patient with a partial PLP1 duplication

Keiko Shimojima[1,2], Takahito Inoue[3], Yuki Imai[4], Yasuhiro Arai[5], Yuta Komoike[6], Midori Sugawara[2], Takako Fujita[3], Hiroshi Ideguchi[3], Sawa Yasumoto[3], Hitoshi Kanno[7], Shinichi Hirose[3] and Toshiyuki Yamamoto[2]

Pelizaeus–Merzbacher disease (PMD) is an X-linked recessive disorder characterized by dysmyelination of the central nervous system (CNS). We identified a rare partial duplication of the proteolipid protein 1 gene (*PLP1*) in a patient with PMD. To assess the underlying effect of this duplication, we examined *PLP1* expression in induced pluripotent stem (iPS) cells generated from the patient's fibroblasts. Disease-specific iPS cells were generated from skin fibroblasts obtained from the indicated PMD patient and two other PMD patients having a 637-kb chromosomal duplication including entire *PLP1* and a novel missense mutation (W212C) of *PLP1*, by transfections of *OCT3/4*, *C-MYC*, *KLF4* and *SOX2* using retro-virus vectors. *PLP1* expressions in the generated iPS cells were examined by northern blot analysis. Although *PLP1* expression was confirmed in iPS cells generated from two patients with the entire *PLP1* duplication and the missense mutation of *PLP1*, iPS cells generated from the patient with the partial *PLP1* duplication manifesting a milder form of PMD showed null expression. This indicated that the underlying effect of the partial *PLP1* duplication identified in this study was different from other *PLP1* alterations including a typical duplication and a missense mutation.
Journal of Human Genetics (2012) **57**, 580–586; doi:10.1038/jhg.2012.71; published online 14 June 2012

Keywords: Pelizaeus–Merzbacher disease (PMD); proteolipid protein 1 gene (*PLP1*); induced pluripotent stem (iPS) cells; partial duplication; dysmyelination

INTRODUCTION

Pelizaeus–Merzbacher disease (PMD; MIM #312080) is an X-linked recessive neurodegenerative disorder characterized by dysmyelination of the central nervous system (CNS). Patients with PMD often present with nystagmus as the initial symptom, and psychomotor developmental delay associated with spasticity and ataxia is seen later in development.[1–3] The proteolipid protein 1 gene (*PLP1*; MIM #300401), located on chromosome Xq22.2, is the gene responsible for PMD. It encodes 2 isoforms, PLP1 and DM20, as a consequence of differential splicing of exon 3. The genetic basis of PMD is unique because two-thirds of *PLP1* abnormalities identified in PMD patients are duplications of small chromosomal segments that include *PLP1*. The remaining one-third of *PLP1* abnormalities are nucleotide alterations in the *PLP1* coding sequence. The nucleotide alterations in *PLP1* are varied and are scattered along the entire coding region of *PLP1*.[1–3]

Because *PLP1* is mainly expressed in oligodendrocytes in the CNS and cultured skin fibroblasts express low levels of *PLP1*, gene expression in the fibroblasts has been analyzed by comparative reverse-transcription (RT)-PCR analysis.[4,5] The use of technology to establish induced pluripotent stem (iPS) cells has now made it possible to examine gene expression and function in greater detail.[6] In 2007, Takahashi *et al.* established iPS cells from human skin fibroblasts.[7] This revolutionary technology has stimulated and accelerated research in embryogenesis and genetics. In this study, we established iPS cells from skin fibroblasts of patients with PMD and examined *PLP1* expression. This is the first report analyzing *PLP1* expression in PMD disease-carrying iPS cells.

MATERIALS AND METHODS

Subjects

For our ongoing study identifying genomic mutations in *PLP1*, three new patients with dysmyelination were referred to us for genetic diagnosis based on the clinical diagnosis of PMD.[8] Clinical information and radiographic findings by MRI for the patients were obtained from attending doctors. Based on

[1]Precursory Research for Embryonic Science and Technology (PRESTO), Japan Science and Technology Agency (JST), Kawaguchi, Japan; [2]Tokyo Women's Medical University Institute for Integrated Medical Sciences, Tokyo, Japan; [3]Department of Pediatrics, School of Medicine, Fukuoka University, Fukuoka, Japan; [4]Department of Pediatrics and Child Health, Nihon University School of Medicine, Tokyo, Japan; [5]Tokyo Metropolitan Tobu Medical Center for Persons with Developmental/Multiple Disabilities, Tokyo, Japan; [6]Department of Hygiene and Public Health, Tokyo Women's Medical University, Tokyo, Japan and [7]Department of Transfusion Medicine and Cell Processing, Tokyo Women's Medical University, Tokyo, Japan
Correspondence: Dr T Yamamoto, Institute for Integrated Medical Sciences, Tokyo Women's Medical University, Kawada-cho 8-1, Shinjuku-ward, Tokyo 162-8666, Japan.
E-mail: yamamoto.toshiyuki@twmu.ac.jp
Received 19 March 2012; revised 15 May 2012; accepted 16 May 2012; published online 14 June 2012

approval by the ethical committees at the institutions, written informed consent was obtained from each patient and/or their family. Peripheral blood samples were collected from the patients and genotyping was performed as described.[8] After genetic diagnosis of PMD was made, another written informed consent for the iPS cell study was obtained from each patient and/or their family. Skin fibroblasts were collected from three patients and a healthy male control.

Genotyping of the patients

Genomic DNAs were extracted from peripheral blood samples from patients and others by using standard methods. Initial screening for *PLP1* duplication was performed by multiplex ligation-dependent probe amplification analysis by using the PLP1 Kit (P022; MRC-Holland, Amsterdam, The Netherlands) according to the manufacturer's instruction.[9] In case of *PLP1* duplication, the aberration region was confirmed by microarray-based comparative genomic hybridization (aCGH) using the Agilent Human 105A CGH Kit (Agilent Technologies, Santa Clara, CA, USA) as described previously.[8] To detect the small duplication in Patient 1, a custom array was designed using e-array, a web-based software (https://earray.chem.agilent.com/earray/), and 29 918 probes in chrX:98 000 000–104 500 000, around *PLP1*, were selected. The average interval of the probes was 217 bp in this region.

PLP1 duplication was confirmed by two-color fluorescence *in-situ* hybridization as described previously.[8] Two bacterial artificial chromosome clones, RP11–75D20 (located at Xp22.13) and RP11–832L2 (located at Xq22.2), were selected from the UCSC Human Genome Browser (http://genome.ucsc.edu/) and used as probes. The fixed metaphase and interphase spreads of the specimens were derived from patients' peripheral blood samples and generated iPS cells. The direction of the duplicated segment identified in Patient 2 was analyzed by fiber-fluorescence *in-situ* hybridization analysis as described previously.[8]

PCR and direct sequencing of all seven exons of *PLP1* was performed by standard methods using the primers reported by Hobson *et al.*[4] The designs of the primers for all exons and the breakpoint searches of the duplicated segments in Patient 1 are listed in Supplementary Table 1.

Cell culture

Human fibroblasts, the Plat-E Retroviral Packaging Cell Line (Cell Biolabs, San Diego, CA, USA), 293FT cells (Life Technologies, Foster City, CA, USA) and mouse fibroblast STO cell line (SNL) feeder cells (ECACC, Salisbury, UK) were grown in Dulbecco's modified Eagle's medium (DMEM 14247-15; Nacalai Tesque, Japan) containing 10% fetal bovine serum and 0.5% penicillin and streptomycin (Life Technologies). Human iPS cells were maintained on SNL feeder cells treated with mitomycin C in Primate ES Cell Culture Medium supplemented with 4 ng ml^{-1} recombinant basic fibroblast growth factor (# RCHEMD001; Repro CELL, Yokohama, Japan) and passaged as described previously.[7,10]

Generation of iPS cells

Disease-specific iPS cells were generated from patients' skin fibroblasts as previously described.[7] Briefly, recombinant lentivirus produced from 293FT cells, in which pLenti6/UbC/mSlc7a1 (AddGene, Cambridge, MA, USA) was transfected by use of Virapower Lentiviral Expression System (Life Technologies), was infected into cultured fibroblasts for 24 h. Then, four retroviruses produced with Plat-E Packaging Cells (Cell biolabs), in which pMXs-hOCT3/4, pMXs-hSOX2, pMXs-hKLF4 and pMXs-hc-MYC (AddGene) were transferred independently, were infected into mSlc7a1-expressing human fibroblasts. Six days after retroviral infection, the fibroblasts were placed onto mouse fibroblast SNL feeder cells (ECACC, Salisbury, UK) at the appropriate concentration. The following day, DMEM 14247-15 (Nacalai Tesque, Japan) was replaced with Primate ES Cell Culture Medium supplemented with 4 ng ml^{-1} recombinant basic fibroblast growth factor (# RCHEMD001; Repro CELL, Yokohama, Japan). Thirty days after transduction, each embryonic stem (ES) cell-like colony was individually placed onto SNL feeder cells. Each colony was tested to determine whether they had indeed acquired pluripotency. After validation,[10] three independent iPS cell clones were selected from the candidates generated from each patient's skin fibroblasts.

Validation of the pluripotency of iPS cells

Initially, alkaline phosphatase staining was performed for validation of iPS cells. Leukocyte Alkaline Phosphatase (AP) kit 86R (Sigma-Aldrich, St Louis, MO, USA) was used for this purpose.

Reactivation of endogenous pluripotency genes and the silencing of artificially induced retroviral transgenes indicated successful reprogramming of putative iPS cell clones. To confirm this, RT-PCR analysis and real-time PCR were performed as described below.

Total RNAs were extracted from iPS cells using ISOGEN (Nippon Gene, Tokyo, Japan) and contaminating genomic DNAs were removed by DNase (Takara, Ohtsu, Japan) according to the manufacturer's instructions. Subsequently, total RNAs were reverse transcribed into complementary DNAs by using the Superscript VILO cDNA Synthesis Kit (Life Technologies) according to the manufacturer's instructions.

Quantitative real-time PCR was performed for *OCT3/4*, *SOX2*, *KLF4*, *C-MYC*, *NANOG*, *REX1*, *GAPDH* and actin beta using the Power SYBR Green PCR Master Mix (Life Technologies) and analyzed with the 7300 Real-Time PCR System (Life Technologies). Primer sequences are shown in Supplementary Table 1.

Immunocytochemistry was also performed for all putative iPS cells. For this purpose, the following primary antibodies were used: anti-SSEA4 (1:200, MAB1435, R&D systems, Minneapolis, MN, USA), anti-OCT3/4 (1:200, AF1759, R&D systems), anti-TRA-1-60 (1:200, MAB4360, Millipore, Billerica, MA, USA), and Anti-TRA-1-81 (1:200, MAB4381, Millipore). Secondary antibodies included Alexa488-conjugated donkey anti-mouse IgG, Alexa488-conjugated goat anti-mouse IgM, and Alexa594-conjugated donkey anti-mouse IgG (1:1000, Life Technologies). Nuclei were stained with Hoechst 33342 (1:1000, Life Technologies).

Validation of the differentiation ability of iPS cells

Determination of the differentiation ability of established iPS cells is important for the selection of putative iPS cell clones. To confirm their pluripotency to differentiate into three embryonic germ layers, we used floating cultivation to form embryoid bodies as described previously.[10] iPS cells were grown as floating cultures for 8 days. After embryoid body formation, the cells were cultured on gelatin-coated dishes for an additional 8 days.

Immunocytochemistry was performed to confirm expression of the three germ layers as described elsewhere.[10] In this case, three primary antibodies were used; anti-βIII tubulin (1:1000, MRB435P, Covance, Princeton, NJ, USA) as the ectoderm marker, anti-α smooth muscle actin (1:200, A2547, Sigma-Aldrich) for mesoderm, and anti-αAFP (1:100, A8452, Sigma-Aldrich) for endoderm. Donkey anti-mouse IgG labeled with Alexa Fluor 594 and donkey anti-rabbit IgG labeled with Alexa Fluor 488 (1:1000, Life Technologies) were used as secondary antibodies. Nuclei were stained with Hoechst 33342 (1:1000, Life Technologies) for nuclear staining.

Validation of the karyotypes of iPS cells

To check the artificial chromosomal rearrangements, conventional G-banding by trypsin treatment stained with Giemsa and aCGH analyses using the same methods described above were performed for the generated iPS cell clones. iPS cell lines that acquired chromosomal rearrangements were eliminated from this study.

Database analysis

Preliminary gene expression analysis was performed using online data sets. Two microarray data sets, GSM242095 for adult human dermal fibroblasts and GSM241846 for iPS cells (clone 201B7),[7] were retrieved from NCBI Gene Expression Omnibus (GEO) and analyzed using GeneSpring GX10 (Agilent Technologies).

Northern blotting

The full-length mRNA of PLP1 (920 bp) and a partial sequence of actin beta (ACTNB; MIM #102630) mRNA (91 bp) were amplified by RT-PCR by using Human Brain Total RNA (#636530, Clonetech, Mountain View, CA, USA) as a template. Primer sequences are listed in Supplementary Table 1. The PCR product was subcloned into pGEM-T Vector System (Promega, Madison, WI,

USA) and grown in LB Broth overnight. Plasmid DNAs were extracted by an automated DNA isolation system, PI-80X (Kurabo, Osaka, Japan). DNA inserts were digested with *Sac*I and *Sac*II restriction enzymes. Following agarose gel electrophoresis, product bands were excised and extracted using the QIAquick Gel Extraction Kit (QIAGEN, Hilden, Germany). The DNA fragments were then labeled using [α-^{32}P] dCTP (PerkinElmer, Waltham, MA, USA) and used as probes for northern blotting.

Hybridization was performed as described previously.[11] Briefly, 30 μg of total RNA was extracted using ISOGEN (Nippon Gene, Tokyo, Japan) according to the manufacturer's instructions, separated on a 1% agarose/0.6 M formaldehyde gel, visualized using Radiant Red RNA Stain (Bio-Rad, Hercules, CA, USA), transferred to a nylon membrane and subsequently hybridized for 24 h with either *PLP1* or *ACTNB* probes. Images were captured using the FLA-5100 scanner (Fujifilm, Tokyo, Japan).

Initial analysis included seven samples: mitomycin-treated and -untreated SNL feeder cells, Epstein-Barr virus-infected immortalized lymphocytes derived from a normal human control, human skin fibroblasts derived from the normal control, iPS cells generated from the normal human control and two brain samples purchased from a provider (Human Fetal Brain Total RNA #636526 and Human Brain Total RNA #636530, Clonetech). Subsequent analysis included the 12 iPS cell lines generated in this study.

RESULTS

Clinical features

Patient 1 was a 16-year-old male, born by spontaneous delivery at 40 weeks gestation, with a weight of 3054 g. Soon after birth he showed nystagmus. At 4 months, he exhibited poor neck control and was diagnosed with spastic paraplegia. Psychomotor development was moderately delayed with walking alone at his age of 2 years and his intelligence quotient was estimated below 50. At 15 years, he was prescribed medication for depression. At that time, his fine motor ability allowed the use of chopsticks but he needed a wheel chair to move. His speech was dysarthric. One month later, he had an epileptic attack and was admitted to the hospital. An electroencephalogram revealed occipital spikes. Although auditory brain response was normal, brain magnetic resonance imaging (MRI) revealed a pattern of mild dysmyelination (Figures 1a and b).

Patient 2 was a 46-year-old male with two healthy female siblings. As he lacked neck control at 1 year of age, he was diagnosed with spastic cerebral palsy. Then, at 4 years, he could turn over but could not sit unaided. He lacked the ability to speak effectively, being limited to two-word sentences. At 15 years, he could use a wheel chair by himself. Subsequently, the quality of his daily life declined gradually. At 39 years, MRI revealed atrophic white matter displaying dysmyelination (Figure 1c). At present, he can move only his upper body very slowly and is bedridden. He is able to comprehend what his siblings say, but he is severely dysarthric and is able to speak only a few words very slowly.

Patient 3 was a 32-month-old boy with a birth weight of 3869 g delivered at 39 weeks gestation. He has a healthy brother. Owing to respiratory problems since birth, he was intubated and tracheostomy was performed at 58 days. He also required tube feeding. He is currently bedridden and has continuous nystagmus. Auditory-brain-response audiometry showed no waves after the first wave. A brain MRI revealed high-intensity lesions of the white matter in a T2-weighted image, indicating severe hypomyelination (Figure 1d).

Molecular analyses

Initial multiplex ligation-dependent probe amplification analysis using a PLP1 Kit (P022; MRC-Holland) identified duplications of *PLP1* in Patient 1 and 2 (data not shown).[9] Patient 2 had a duplication of all 7 exons of *PLP1*, and subsequent aCGH analysis

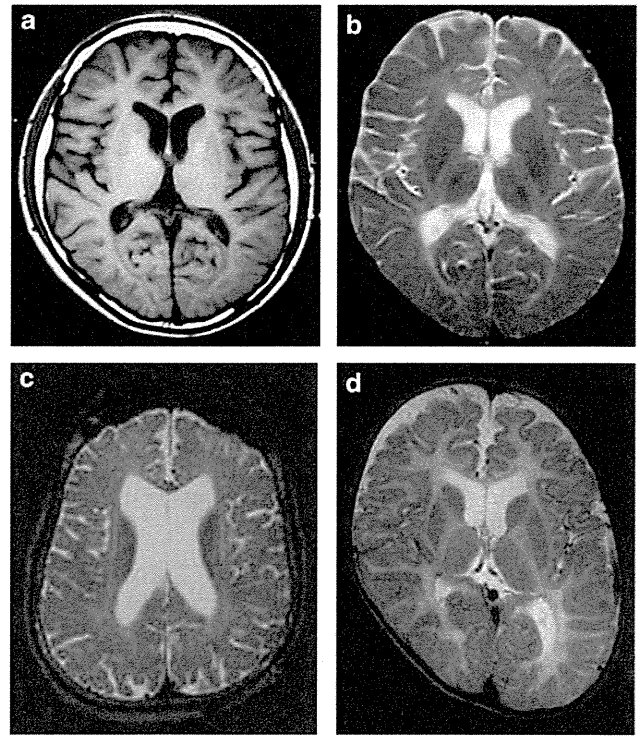

Figure 1 Brain MRI findings of the patients T1- (**a**) and T2 (**b**) weighted images of Patient 1 show mild and diffuse volume loss of the brain and high-intensity signals of the deep white matter in T2 indicating mild dysmyelination. T2-weighted image of Patient 2 (**c**) shows diffuse volume loss resulting in the dilatation of the ventricles and dysmyelination in the white matter. T2-weighted image of Patient 3 (**d**) shows extremely hypomyelinated pattern with high intensity in all white matter.

by using the Human Genome CGH Microarray 105 K (Agilent Technologies) revealed that the duplicated region was chrX:102 519 000–103 155 851 (636 851 bp) with an average $\log_2$ ratio of +0.83, which is a typical duplication region seen in PMD patients with *PLP1* duplications (Figure 2a). The duplication was confirmed by fluorescence *in-situ* hybridization (Figure 2b), and the direction of the duplicated segment, including *PLP1*, was shown to be in a tandem configuration by fiber-fluorescence *in-situ* hybridization analysis (Figure 2c).

The duplication identified in Patient 1 was unique because only the first 3 exons (exons 1–3) of *PLP1* were included in the duplicated region. To confirm this partial duplication, we designed a custom aCGH chip and used it to detect the precise duplication region. As shown in Figure 3a, the duplicated region was chrX:102 912 361–102 928 360 (15 999 bp) with an average $\log_2$ ratio of +0.72. To determine the location of the duplicated segment, we sought to detect the breakpoint by PCR direct sequencing, using primers A and B (Supplementary Table 1). A 775-bp band was obtained and re-sequenced (Figures 3b and c). Ultimately, an extremely small duplication of 16 208 bp, which has never been previously reported, was identified. The sample from Patient 1's mother was also analyzed and she was found to be a carrier of this duplication (Figures 3b and c).

In Patient 3, a novel missense mutation, c.636G>C (W212C), was identified in exon 5 of *PLP1* (Figure 2d). The *PLP1* sequence is completely conserved among species and this novel mutation was not identified in 100 normal control samples (50 males and 50 females). This patient's mother declined to have her genotype analyzed.

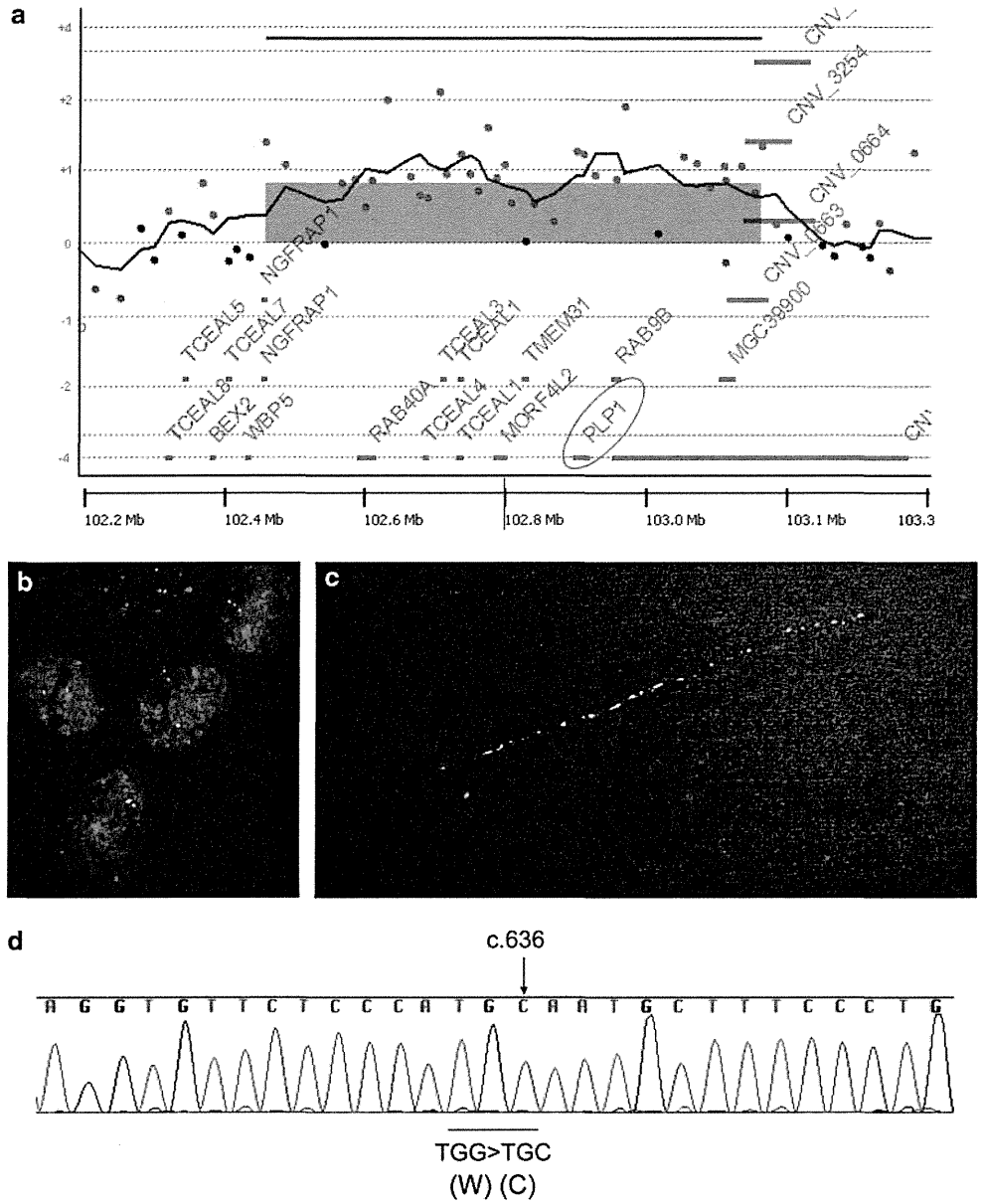

Figure 2 Genotyping and cytogenetic analyses for Patients 2 and 3. (**a**) A microchromosomal duplication including *PLP1* is shown in GeneView of Agilent Genomic Workbench (Agilent Technologies). The location of *PLP1* is highlighted by a red circle. (**b**) Interphase fluorescence *in-situ* hybridization analysis shows two green signals labeled on RP11-832L2 (located at Xq22.2) in the nucleus. Red signals labeled on RP11-75D20 (located at Xp22.13) are the marker for X chromosome. (**c**) Fiber-fluorescence *in-situ* hybridization analysis indicates tandem configuration of the duplicated segments labeled with green and red probes. (**d**) Electropherogram shows a novel missense mutation c.636G>C (W212C) in Patient 3.

Generation of iPS cells

We successfully generated iPS cells from three patients with PMD and a normal male control (Supplementary Figure 1). At least three independent clones were validated using the following three categories: (1) silencing of four transfected genes (*OCT3/4, C-MYC, KLF4* and *SOX2*; Supplementary Figure 2); (2) expression of endogenous pluripotency genes (*OCT3/4, SOX2, KLF4, C-MYC, NANOG* and *REX1*; Supplementary Figures 3 and 5); and (3) confirmation of the differentiation potency by immunocytochemistry (Supplementary Figure 4). Karyotype and aCGH analyses for the resulting iPS cells showed no artificial chromosomal rearrangements.

PLP1 expression

Preliminary *PLP1* expression levels were compared between two online data sets for human skin fibroblasts and iPS cells. The results showed that *PLP1* expression levels were $\times 40.70$ ($\log_2 = 6.38$) higher in iPS cells than in skin fibroblasts (Supplementary Figure 6). Subsequently, our initial experiments for *PLP1* expression in several samples were performed by northern blot analysis, which revealed predominant *PLP1* expression in the brain (fetal brain had weaker expression than adult brain). Although the other samples showed no *PLP1* expression, we could detect the *PLP1* band in iPS cells (Figure 4); the differentiation between two isoforms for *PLP1* and *DM20* could not be detected owing to small size differences as same as

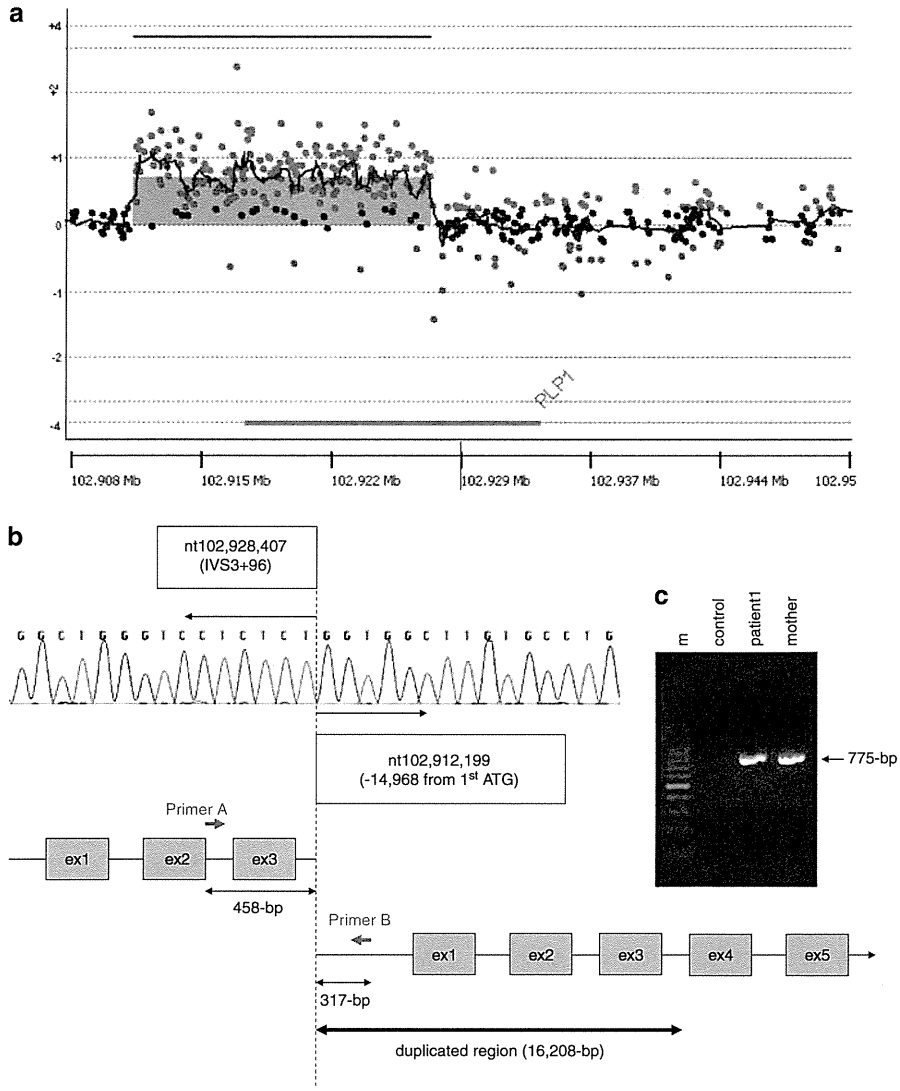

Figure 3 Molecular analyses of the *PLP1* duplication identified in Patient 1. (**a**) The result of a custom-designed aCGH shows partial duplication of *PLP1*. (**b**) A schematic representation of the breakpoint analyzed by PCR and subsequent sequencing. (**c**) A 775 bp PCR product including a breakpoint is amplified by Primer A and B and is shown in electrophoresis. m; molecular marker OneSTEP Ladder 50 (Nippon Gene).

the previous study.[12] Finally, total RNA samples extracted from the 12 iPS cell clones generated in this study were analyzed. Although we could detect the *PLP1* band in iPS cells from normal individual and Patients 2 and 3, we could not detect the *PLP1* band in the iPS cells generated from Patient 1, indicating null expression of *PLP1* caused by the partial duplication of *PLP1* (Figure 5). In Patients 2 and 3, *PLP1* signals appeared to be somewhat stronger than in controls, but because of the large variation in signal intensity among different cell lines, it was inconclusive in our limited experiments.

DISCUSSION

In this study, we identified different *PLP1* abnormalities in three patients with PMD. Patient 3 showed a novel missense mutation, c.636G>C (Tyr212Cys), which is in the extramembrane region of the PLP1 protein.[2] A missense substitution in the same codon, but resulting in a change into a different amino acid, c.634T>C (Tyr212Arg), has been reported to be a pathogenetic mutation by others.[13] Frequently, a cysteine residue changes the three-dimensional protein conformation drastically owing to disulfide bond formation with other cysteines.[14] Thus, the amino-acid substitution to cysteine in our patient is likely a pathogenetic mutation, causing PMD. Previous genotype-phenotype correlation study showed that the phenotype of patients with *PLP1* missense mutations was more severe than those with *PLP1* duplications.[1–3] Indeed, Patient 3 showed severely delayed psychomotor development complicated by respiratory and feeding difficulties. His condition can be classified as form 0 according to the classification proposed by Cailloux *et al.*,[13] as form 0 is the most severe form of PMD. Dysmyelination in this patient was particularly severe.

Patient 2 had a 0.6-Mb duplication including *PLP1*. This size is typical for PMD patients with *PLP1* duplications.[8,15,16] This patient is now 43 years old and does not show any deterioration of neurological abilities. Despite being bedridden, he can verbally communicate with several words. His clinical condition can be classified as form 2, because his maximum motor ability was sitting. His dysmyelination is milder than that of Patient 3.

The most intriguing result in this study is the partial duplication of *PLP1* identified in Patient 1. Although there have been reports

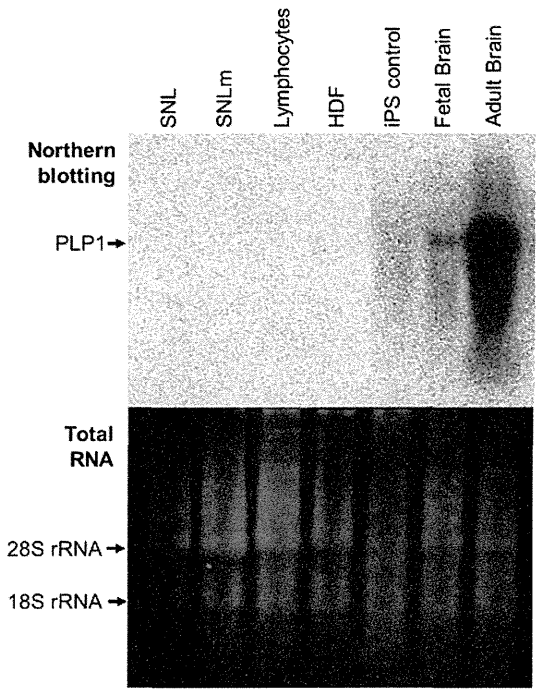

Figure 4 *PLP1* expression analysis by the northern blotting for various samples. (Upper) Predominant expression of *PLP1* is shown in the brain samples. Although control iPS cells show weak expression, there are no expressions of *PLP1* in the other samples. (Bottom) Agarose gel staining for the total RNAs before subsequent northern blotting indicates the same amounts of total RNAs loaded in each lane. SNLm, SNL-feader cells treated with mitomycin; HDF, human dermal fibroblasts

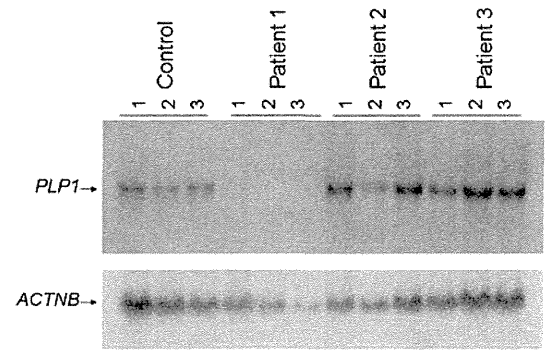

Figure 5 *PLP1* expression analyses using northern blotting. Three iPS cells of Patient 1 show no *PLP1* band, whereas the other iPS cells from normal control, Patient 2 and Patient 3 show expressions of *PLP1*. *ACTNB* (actin beta) is used for internal control.

of partial deletions in *PLP1* identified by multiplex ligation-dependent probe amplification analysis,[9] this is the first report of a partial duplication of *PLP1*. The duplicated segment included the promoter region and the first three exons. Therefore, we hypothesized that a very short mRNA or long fusion mRNA might be expressed by this duplication together with the normal mRNA. To confirm this hypothesis, we analyzed *PLP1* expression by using northern blot analysis, the only way to detect the length and the quantity of mRNAs. As expression levels of *PLP1* in skin fibroblasts were too low to be examined by northern blot analysis, we generated iPS cells from the patients. Contrary to expectation, northern blot analysis showed no *PLP1* bands in the iPS cell generated from the fibroblasts of Patient 1. Although there may be a limitation to detect short-unstable mRNAs in our method, this possibly indicated that the expression of *PLP1* mRNA was disturbed by the *PLP1* partial duplication identified in Patient 1. Regarding the clinical severities of the patients, Patient 1 showed milder phenotype than Patient 2, and his condition can be classified as form 3. Previous genotype-phenotype correlation study have shown that patients with *PLP1* missense mutations show severe manifestation associated with severe hypomyelination, which is recognized as the consequence of accumulated mutant protein in the endoplasmic reticulum as a gain-of-toxic function of the mutant protein.[2] Excessive PLP1 protein resulting from genomic duplications may accumulate in late endosomes/lysosomes, promoting its incorporation into other myelin components.[1] In contrast, patients with *PLP1* null mutations escape severe impairments because of the absence of any gain-of-toxic function.[2,13,17] Indeed, knockout mice with a functionally null *Plp1* gene do not develop classical signs of *Plp1*-related disease; their oligodendrocytes develop normally and synthesize compact myelin sheaths.[3,18] However, the mice show ultrastructural abnormalities, including swelling of the small-diameter axons and late-onset axonal degeneration.[3,19] Consequently, a loss-of-function mutation of *PLP1* does not induce oligodendrocyte cell death, possibly serving as a mechanism underlying the milder phenotypic consequences observed in patients with null *PLP1* mutations. Although length-dependent axonal degeneration has been described in *PLP1* null mutations,[20] there is no information about peripheral neuropathy in Patient 1. Thus, it was unclear whether the clinical condition of Patient 1 is compatible with that of *PLP1* null mutations. However, the lack of *PLP1* expression in iPS cells derived from Patient 1 clearly demonstrated that the underlying mechanism of PMD in Patient 1, with a partial *PLP1* duplication, is different from the other two patients in this study.

Immortalized lymphocytes and skin fibroblasts derived from patients are often used for expression studies or biological analyses, as these cells are easy to be obtained and handled. However, many tissue-specific genes are not sufficiently expressed by these cells; *PLP1* being one of them. Although there are reports examining *PLP1* expression by RT–PCR, using mRNA extracted from skin fibroblasts,[4,5,21] the expression of *PLP1* mRNA in skin fibroblasts is too low to be examined by northern blotting as shown here. In this study, our microarray database search showed over 40 times higher *PLP1* expression in iPS cells than that in skin fibroblasts. Our initial northern blot analysis confirmed faint but detectable *PLP1* expression in iPS cells, whereas no expression was observed in skin fibroblasts, lymphocytes or SNL feeder cells. This study also confirmed a lack of *PLP1* expression in SNL feeder cells. Therefore, this study demonstrates that iPS cells express endogenous *PLP1*, and that the possibility of contamination from SNL feeder cells or original skin fibroblasts can be excluded. Although being detectable by northern blotting, *PLP1* expression in iPS cells appeared to be much lower than that in mature oligodendrocytes and may be simply cryptic rather than functional. If so, this allows us to evaluate the native transcriptional level of each mutant (and wild-type) *PLP1* allele, which is the primary focus of our study. Meanwhile, terminal differentiation of iPS cells into the oligodendrocyte lineage would result in an enhanced *PLP1* expression with functional consequence. However, this requires technological breakthrough in the induction of terminal differentiation into oligodendrocyte lineage, which is currently unavailable.

In conclusion, we identified the first PMD patient having a partial *PLP1* duplication. The absence of *PLP1* expression in iPS cells, generated from the patient's skin fibroblasts, proved the underlying effects of the partial *PLP1* duplication for the PMD development.

CONFLICT OF INTEREST

The authors declare no conflict of interest.

ACKNOWLEDGEMENTS

We thank the patients and their families for their cooperation. This work was mainly supported by JST PRESTO program (KS) and was partially supported by Grant-in-Aid for Scientific Research on Innovated Areas 'Foundation of Synapse and Neurocircuit Pathology' and Grant-in-Aid for scientific research from Health Labor Sciences Research Grants from the Ministry of Health, Labor and Welfare, Japan (TY). This work was supported in part by Grant-in-Aid for Scientific Research (A) 21249062, Japan Society for the Promotion of Science (JSPS) and 'High-Tech Research Center' Project for Private Universities: matching fund subsidy from the Ministry of Education, Culture, Sports, Science and Technology, 2006–2010 'The Research Center for the Molecular Pathomechanisms of Epilepsy, Fukuoka University', Research Grants (21B-5) for Nervous and Mental Disorder from the Ministry of Health, Labor and Welfare and Health and Labor Science Research Grant 21210301, KB220001 from the Ministry of Health, Labor and Welfare, and Adaptable and Seamless Technology Transfer Program through Target-driven R&D (A-STEP) Exploratory Research, Japan Science and Technology Agency (JSP) (SH). KS thanks Hayashi Memorial Foundation for Female Natural Scientists for grant aid support.

WEB SITE: NCBI GEO; http://www.ncbi.nlm.nih.gov/guide/genes-expression/ OMIM; http://omim.org/

1 Inoue, K. PLP1-related inherited dysmyelinating disorders: Pelizaeus-Merzbacher disease and spastic paraplegia type 2. *Neurogenetics* **6,** 1–16 (2005).
2 Garbern, J.Y. Pelizaeus-Merzbacher disease: Genetic and cellular pathogenesis. *Cell. Mol. Life Sci.* **64,** 50–65 (2007).
3 Woodward, K.J. The molecular and cellular defects underlying Pelizaeus-Merzbacher disease. *Expert. Rev. Mol. Med.* **10,** e14 (2008).
4 Hobson, G.M., Huang, Z., Sperle, K., Sistermans, E., Rogan, P.K., Garbern, J.Y. *et al.* Splice-site contribution in alternative splicing of PLP1 and DM20: molecular studies in oligodendrocytes. *Hum. Mutat.* **27,** 69–77 (2006).
5 Regis, S., Grossi, S., Corsolini, F., Biancheri, R. & Filocamo, M. PLP1 gene duplication causes overexpression and alteration of the PLP/DM20 splicing balance in fibroblasts from Pelizaeus-Merzbacher disease patients. *Biochim. Biophys. Acta.* **1792,** 548–554 (2009).
6 Inoue, H. Neurodegenerative disease-specific induced pluripotent stem cell research. *Exp. Cell. Res.* **316,** 2560–2564 (2010).
7 Takahashi, K., Tanabe, K., Ohnuki, M., Narita, M., Ichisaka, T., Tomoda, K. *et al.* Induction of pluripotent stem cells from adult human fibroblasts by defined factors. *Cell* **131,** 861–872 (2007).
8 Shimojima, K., Inoue, T., Hoshino, A., Kakiuchi, S., Watanabe, Y., Sasaki, M. *et al.* Comprehensive genetic analyses of PLP1 in patients with Pelizaeus-Merzbacher disease applied by array-CGH and fiber-FISH analyses identified new mutations and variable sizes of duplications. *Brain Dev.* **32,** 171–179 (2010).
9 Warshawsky, I., Chernova, O.B., Hubner, C.A., Stindl, R., Henneke, M., Gal, A. *et al.* Multiplex ligation-dependent probe amplification for rapid detection of proteolipid protein 1 gene duplications and deletions in affected males and carrier females with Pelizaeus-Merzbacher disease. *Clin. Chem.* **52,** 1267–1275 (2006).
10 Ohnuki, M., Takahashi, K. & Yamanaka, S. Generation and characterization of human induced pluripotent stem cells. *Curr. Protoc. Stem Cell Biol.* Chapter 4, Unit 4A2 (2009).
11 Yamamoto, T., Feng, J.H., Higaki, K., Taniguchi, M., Nanba, E., Ninomiya, H. *et al.* Increased NPC1 mRNA in skin fibroblasts from Niemann-Pick disease type C patients. *Brain Dev.* **26,** 245–250 (2004).
12 Iwaki, A., Muramoto, T., Iwaki, I., Furumi, H., Dario-deLeon, M.L., Tateishi, J. *et al.* A missense mutation in the proteolipid protein gene responsible for Pelizaeus-Merzbacher disease in a Japanese family. *Hum. Mol. Genet.* **2,** 19–22 (1993).
13 Cailloux, F., Gauthier-Barichard, F., Mimault, C., Isabelle, V., Courtois, V., Giraud, G. *et al.* Genotype-phenotype correlation in inherited brain myelination defects due to proteolipid protein gene mutations. Clinical European Network on Brain Dysmyelinating Disease. *Eur. J. Hum. Genet.* **8,** 837–845 (2000).
14 Dhaunchak, A.S. & Nave, K.A. A common mechanism of PLP/DM20 misfolding causes cysteine-mediated endoplasmic reticulum retention in oligodendrocytes and Pelizaeus-Merzbacher disease. *Proc. Natl Acad. Sci. USA* **104,** 17813–17818 (2007).
15 Lee, J.A., Inoue, K., Cheung, S.W., Shaw, C.A., Stankiewicz, P. & Lupski, J.R. Role of genomic architecture in PLP1 duplication causing Pelizaeus-Merzbacher disease. *Hum. Mol. Genet.* **15,** 2250–2265 (2006).
16 Woodward, K.J., Cundall, M., Sperle, K., Sistermans, E.A., Ross, M., Howell, G. *et al.* Heterogeneous duplications in patients with Pelizaeus-Merzbacher disease suggest a mechanism of coupled homologous and nonhomologous recombination. *Am. J. Hum. Genet.* **77,** 966–987 (2005).
17 Sistermans, E.A., de Wijs, I.J., de Coo, R.F., Smit, L.M., Menko, F.H. & van Oost, B.A. A (G-to-A) mutation in the initiation codon of the proteolipid protein gene causing a relatively mild form of Pelizaeus-Merzbacher disease in a Dutch family. *Hum. Genet.* **97,** 337–339 (1996).
18 Klugmann, M., Schwab, M.H., Puhlhofer, A., Schneider, A., Zimmermann, F., Griffiths, I.R. *et al.* Assembly of CNS myelin in the absence of proteolipid protein. *Neuron* **18,** 59–70 (1997).
19 Griffiths, I., Klugmann, M., Anderson, T., Yool, D., Thomson, C., Schwab, M.H. *et al.* Axonal swellings and degeneration in mice lacking the major proteolipid of myelin. *Science* **280,** 1610–1613 (1998).
20 Garbern, J.Y., Yool, D.A., Moore, G.J., Wilds, I.B., Faulk, M.W., Klugmann, M. *et al.* Patients lacking the major CNS myelin protein, proteolipid protein 1, develop length-dependent axonal degeneration in the absence of demyelination and inflammation. *Brain* **125,** 551–561 (2002).
21 Mikesova, E., Barankova, L., Sakmaryova, I., Tatarkova, I. & Seeman, P. Quantitative multiplex real-time PCR for detection of PLP1 gene duplications in Pelizaeus-Merzbacher patients. *Genet. Test.* **10,** 215–220 (2006).

Supplementary Information accompanies the paper on Journal of Human Genetics website (http://www.nature.com/jhg)

J. Spine Res. 3 : 1470-1474, 2012

原著 Original Article

肋骨異常を合併した先天性側弯症：成長期における自然経過の検討

Radiographic Analysis of Progression in Congenital Scoliosis (CS) with Rib Anomalies (RA) during Growth Period

川上紀明[*1] 辻 太一[*1] 柳田晴久[*2] 宇野耕吉[*3]
松本守雄[*4] 渡辺航太[*4] 山元拓哉[*5] 平野 徹[*6]
種市 洋[*7] 山崎 健[*8] 藤原憲太[*9]

Noriaki Kawakami[*1], Taichi Tsuji[*1], Haruhisa Yanagida[*2], Kouki Uno[*3], Morio Matsumoto[*4], Kota Watanabe[*4], Takuya Yamamoto[*5], Toru Hirano[*6], Hiroshi Taneichi[*7], Ken Yamazaki[*8], Kenta Hujiwara[*9]

要 旨

肋骨異常を合併した先天性側弯症の成長期における自然経過を明らかにする目的で70例の臨床データーを成長時期別に検討した．側弯は乳幼児期に最も悪化し，思春期がその次に続く結果であった．この悪化には肋骨変形が片側性，片側分節異常を伴う混合型の奇形椎，肋骨癒合/肋骨欠損などが存在する，広範囲な肋骨異常，などが大きく関与していた．この結果を加味して，手術時期を判断する目的で4段階の重症度分類を提唱した．

Abstract

Introduction：This study was aimed to evaluate the progression of various types of CS with RA during each of the growth periods, and to assess the severity of progression for strategic planning of expansion thoracoplasty (ET).

Material & Methods：70 pts. (M-32 and F-38 with an average age of 2.6 years at the first visit.) from 13 institutions matched the inclusion criteria：CS with RA, no procedures that could influence the natural history, repeated plain X-ray check-ups at at least a 2-year interval during growth periods. The average F/U time was 5.4 years (2-14). X-ray images of 70 pts. were divided into 3 age groups, infantile (0-6), juvenile (5-11), and adolescent (11-18).

Results：54 of 70 pts. had unilateral RA. The magnitude of scoliosis was 49.3° at the first visit and 65.7° at the final F/U. Scoliosis progressed most severely during infancy with the rate of 5.9°/y, followed by 3.9°/y during adolescence. Patients with rib defects or unilateral unsegmented bar showed higher progression rates during infancy. 4 grades in severity of progression (most severe.

[*1]国家公務員共済組合連合会名城病院整形外科脊椎脊髄センター〔〒460-0001 名古屋市中区三の丸1-3-1〕Department of Orthopedic Surgery, Meijo Hospital
[*2]福岡市立こども医療センター整形外科
[*3]独立医療法人神戸医療センター整形外科
[*4]慶應義塾大学医学部整形外科
[*5]鹿児島大学医学部整形外科
[*6]新潟大学医学部整形外科
[*7]獨協医科大学整形外科
[*8]岩手医科大学整形外科
[*9]大阪医科大学整形外科

severe, moderate, mild) were set up based on the relationship between SAL and scoliosis with cut-off values of 70%, 85% of SAL and 45°, 85° of scoliosis. Those grades were significantly related with types and location of RA and types of vertebral anomalies. [Conclusion] Scoliosis in CS with RA progressed most severely during infancy and was significantly related to the types and location of RA as well as the type of VA.

Key words：congenital scoliosis, congenital rib anomalies natural history

はじめに

幼少児期に高度に悪化する脊柱変形[1)2)]の中でも先天性に肋骨と脊柱の両方に生じる異常は胸郭不全症候群の代表的疾患であり，成長障害も加わり胸郭の三次元的変形と低形成，脊柱側弯や後弯・前弯などにより外見のみならず拘束性換気障害を来たし致死的となるものも認められる．しかし，Ramirez ら[3)]，Tsiricos ら[4)]の報告はあるものの，未だ本疾患群に対する自然経過の実態把握は不十分であり，どのような病態が胸郭不全症候群と言えるのかなど，悪化因子や治療成績に関係する様々な病態が十分解明されていない．また，成長に大きく影響されるため成長終了以前の早期に診断する診断基準が存在せず，治療方法に対するガイドラインも存在していない．平成21年以後，われわれは全国実態調査により自然経過や治療状況，悪化因子などを検討し，過去の治療の問題点と限界を検討してきた．その結果を2011年に本誌において肋骨異常を伴う先天性側弯症：その悪化因子として報告した[5)]．しかし，対象とした症例の年齢が様々であり，成長時期の影響が全く考慮されていないという問題点があった．

本研究の目的は先天性側弯症の中で肋骨異常のある疾患の自然経過，病態をさらに詳細に調査することにより本疾患のそれぞれの成長時期における悪化状態とそれらに影響を与える因子を解明し，重症度を明確にすることである．

対象と方法

臨床データーを retrospective に調査検討した．2010年に行った本疾患におけるアンケート調査に対して回答のあった施設から，複数回の診察により経過観察が行われていた症例を有する13施設から患者情報，X線写真の提供を受け検討した．対象症例は，未成熟な患者，肋骨異常を伴う先天性側弯症，手術治療なしで最低2年間自然経過を観察できたものとし，医原性のものは除外した．

提供を受けた症例を以下のごとく3群に分けて検討した．

1）生下時から5～6歳まで経過を観察(乳幼児期)

2）5～6歳から10～11歳まで経過を観察(学童期)

3）11歳以後18歳未満で経過を観察(思春期)

それぞれの症例において初診時，経過観察時のX線写真(全脊柱正面，側面，あれば3DCT)，呼吸状態，全身状態を評価し，X線画像に対しては，肋骨・脊椎の変形と側弯(変形)の進行との関係を検討した．

結　果

13医療機関から提供された症例中から上記症例選択基準にマッチした70患者(男性32名，女性38名)を対象とした．これらの患者の初診時年齢は平均2.6±3.5歳(0～13.6歳)，経過観察期間は5.4±3.4年(2～14年)であった．初診時の側弯は46.9±26.0°であったが，最終観察時65.7±30.7°まで進行していた($p<0.001$)．

1．成長時期と側弯の悪化の検討

乳幼児期の症例では立位歩行が不可能な時期と立位可能になってからのX線画像には重力の影響が大きく影響しているため，臥位での乳幼児期と立位可能な幼児期のサブグループに分けて検討した．その結果，年齢，症例数，側弯 Cobb 角はそ

表1　各年代別の悪化速度

	乳幼児期	幼児期	学童期	思春期
年齢	1.1±1.0 (0～3)	4.3±1.2 (2～7)	8.9±2.0 (6～13)	14.1±2.0 (11～19)
症例数	55	61	39	24
側弯 Cobb 角	47.3±23.0	58.4±29.7	56.2±30.7	72.0±30.5
進行度	5.0±5.6	2.3±2.1	3.8±2.2	

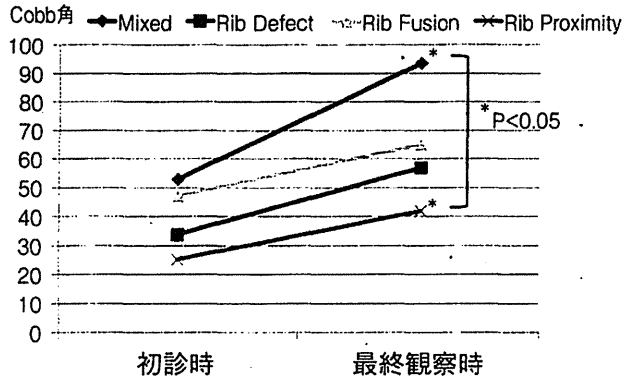

図2　側弯の大きさと肋骨奇形のタイプ
側弯は肋骨の異常が混合型，肋骨癒合，肋骨欠損，肋骨近接，の順で大きかった．特に混合型と近接には統計的有意差があった．

れぞれ乳幼児期で1.1±1.0歳，55例，47.3±23.0°，幼児期で4.3±1.2歳，61例，58.4±29.7°，学童期で8.9±2.0歳，39例，56.2±30.7°，思春期で14.1±2.0歳，24例，72.0±30.5°となっていた(表1)．進行度は乳幼児期から幼児期で5.0±5.6°/年，幼児期から学童期で2.3±2.1°/年，学童期から思春期で3.8±2.2°/年となっており，乳幼児期で最も悪化していた．特に臥位から立位への移行期における重力の影響を考慮した22例の検討では，初診時年齢0.2±0.3歳，側弯 Cobb 角52.8±24.6°が立位歩行開始後最初の X 線撮影時それぞれ2.1±0.9歳，67.5±29.4°となっており，7.8±7.0°/年の最も大きい進行度を示していた．

2．肋骨奇形の部位・範囲と側弯角度

70例中54例は片側のみに肋骨異常があり，16例は両側性であった．片側性と両側性の初診時 Cobb 角と最終時 Cobb 角には有意差があったが，悪化度には有意差はなかった(図1)．肋骨異常のタイプは，52例が肋骨癒合で，単純 X 線写真では

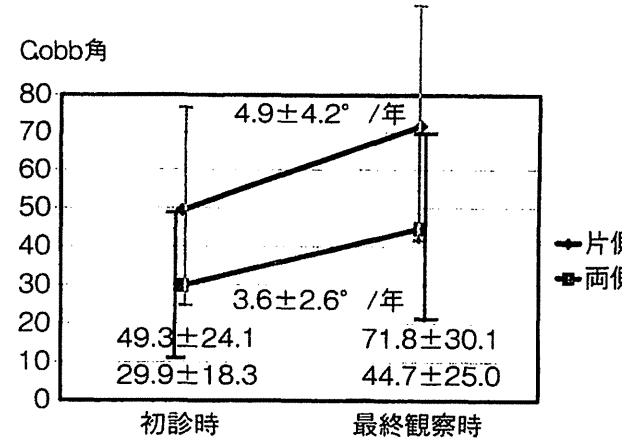

図1　側弯と肋骨異常のタイプ(片側性と両側性)
肋骨異常が片側性でも両側性でも経過観察期間内で側弯は悪化したが両者に統計的有意差はなかった．片側性の症例の方が側弯の角度は有意に高かった．

癒合が明確でなく近接していたもの8例，肋骨欠損4例であった．欠損と癒合の混合したものは6例認められた．側弯の大きさは混合型，癒合，欠損，近接の順で大きく，進行度では混合，欠損，癒合，近接の順であった(図2)．肋骨異常の部位は全体を3等分して上位，中位，下位に分けて検討した．全体の2/3以上にわたって異常を認めた症例は45例(全体-15，上位2/3-16，下位2/3-14)であり，肋骨異常が広範囲に存在する症例ほど側弯が大きかった．

3．片側のみに肋骨異常を伴う症例の検討(54例)

初診時年齢は平均2.6±3.6歳，側弯は49.3±24.1°であり，最終観察時では8.7±5.0歳，側弯は65.7±30.7°まで進行していた．側弯進行度は乳幼児期で5.9±7.6°/年，学童期で2.5±2.0°/年，思春期で3.9±2.3°/年となっており，乳幼児期での進行が大きかった(p=0.02)．肋骨異常のタイプと側弯の悪化には優位な関係は認めなかったが，肋骨欠損の有無での検討では有の症例では7.3±5.6°/年と明らかに無の症例の4.3±3.6°/年よりも進行性であった．特にその中でも乳幼児期の進行度には大きな差が認められた(有－10.7±1.8°/年，無－3.8±0.9°/年)．奇形椎のタイプと側弯進行度とは症例数にあまりに差があり有意な関係は認めなかったが，明らかに混合型の進行度が高かった．

表2　混合型における片側癒合の側弯悪化に対する影響

	側弯悪化率	初診時 Cobb 角	最終観察時 Cobb 角
UUB(＋)	7.2±5.1	58.5±21.8	88.8±21.6
UUB(－)	3.2±2.6	46.4±23.1	61.0±31.6
	p=0.0032	p=0.0864	P=0.0017

表3　分節異常における片側癒合の側弯悪化に対する影響

	側弯悪化率	初診時 Cobb 角	最終観察時 Cobb 角
UUB(＋)	3.6±2.8	44.1±24.9	64.8±27.1
UUB(－)	2.6±2.8	10.5±3.5	34.0±31.1
	p=0.6331	p=0.1008	P=0.1876

表4　肋骨異常の範囲と側弯の悪化

肋骨癒合の範囲	症例数	悪化率(°/年)
ほぼ全範囲	11	7.5±6.0*
2/3前後	20	5.1±6.4
1/3前後	23	3.5±3.2*

All pairs Tukey-Kramer 0.05
*p=0.0306

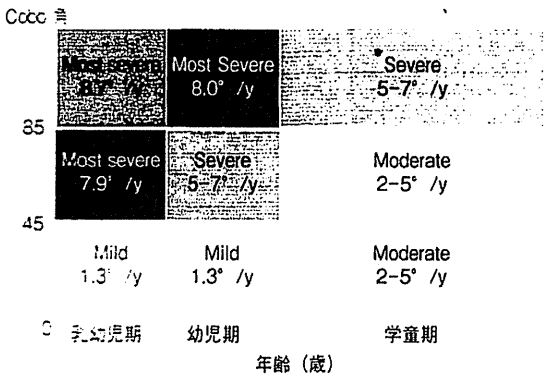

図4　成長期における側弯の悪化
成長時期における Cobb 角の大きさと悪化率の関係では，より幼少児期で側弯が高度であればあるほど側弯は高度に悪化していた．

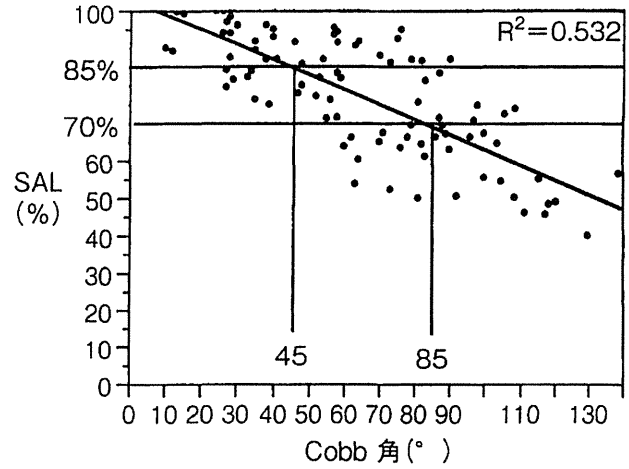

図3　側弯の角度と SAL
70例における SAL と側弯角度の関係は負の相関関係にあり(R^2=0.532)，SAL の85%，70%がそれぞれ側弯角度の45度，85度に一致していた．

特に，片側癒合(unilateral unsegmented bar，以下 UUB)の有無でその進行度を評価すると，有の症例では6.2±0.7°/年と明らかに無の症例の3.2±0.8°/年よりも大きく進行していた．UUB は混合型と分節異常の両方に認められたが，混合型で UUB が合併した症例の方が分節異常における UUB よりも優位に進行度が大きかった(表2，3)．肋骨異常の範囲と側弯の進行の関係では，全範囲，2/3以上に肋骨異常を伴った症例では明らかにそれ以下よりも高度に悪化していた(表4)

4．両側肋骨癒合の症例における検討

初診時年齢は平均2.9±3.0歳，側弯は29.9±18.3°であり，最終観察時では6.8±3.8歳，側弯は44.7±21.5°まで進行していた．側弯進行度は乳幼児期で3.7±2.9°/年，学童期で2.2±2.1°/年，思春期で3.9±2.1°/年となっており，統計学的有意差は認められなかった．

5．側弯 Cobb 角と SAL，THR の関係

胸郭の左右対称性を表す SAL(Space Available for Lung)は経過観察期間中大きな変化はなく，胸椎から腰椎までの高さと胸椎の高さとの比 THR (Thoracic Height Ratio)にも有意差は存在しなかった．しかし，SAL と側弯の大きさとの相関関係は r^2=0.532と有意に負の相関関係を示し，側弯が45°で SAL は85%，側弯が85°で SAL は70%となり，胸郭変形と側弯の両方の観点から手術適応を検討する上で大変重要な境界値になると考えられた(図3)．側弯の大きさと各年代に分けて側弯の悪化率を整理すると図4のようになり，乳幼児期で側弯角度が85度以上となった症例で最も悪化速